



12-2019

Gearbox Baffle Optimization

Megan Arduin
Western Michigan University

Follow this and additional works at: https://scholarworks.wmich.edu/masters_theses



Part of the Mechanical Engineering Commons

Recommended Citation

Arduin, Megan, "Gearbox Baffle Optimization" (2019). *Masters Theses*. 5091.
https://scholarworks.wmich.edu/masters_theses/5091

This Masters Thesis-Open Access is brought to you for free and open access by the Graduate College at ScholarWorks at WMU. It has been accepted for inclusion in Masters Theses by an authorized administrator of ScholarWorks at WMU. For more information, please contact wmu-scholarworks@wmich.edu.



GEARBOX BAFFLE OPTIMIZATION

by

Megan Arduin

A thesis submitted to the Graduate College in
partial fulfillment of the requirements for the
degree of Master of Science in Engineering
Mechanical Engineering
Western Michigan University
December 2019

Thesis Committee:

Richard T. Meyer, Ph.D., P.E.,
Chair Claudia Fajardo-Hansford,
Ph.D. William W. Liou, Ph.D.

Copyright by
Megan Arduin
2019

ACKNOWLEDGEMENTS

I would like to acknowledge the people that took the time to discuss with me different factors of simulation Dr. Yang Yang and Dr. William Liou. Secondly, I would like to thank the members of my graduate committee for taking the time to review my work, Dr. Richard Meyer, Dr. Claudia Fajardo, and Dr. William Liou. I would like to thank Dr. Richard Meyer and Dr. Claudia Fajardo in particular for their continued help with keeping this research on track. I would also like to thank the CAViDS program at Western Michigan University for their sponsorship of this research.

Lastly, I would like to thank my family and friends for their continued support while working on this thesis.

Megan Arduin

GEARBOX BAFFLE OPTIMIZATION

Megan Arduin, M.S.E.

Western Michigan University, 2019

Current literature reveals there is limited consensus on the placement of baffles within a gearbox to reduce churning losses. Thus, there is a need for a process to identify baffle clearances that result in maximum and minimum churning losses. There are two types of baffles: axial and radial. While both axial and radial baffles cause reductions in churning losses to various degrees, the focus is on the effect of radial baffles. The effect of a board (rectangular plate) baffle location on the churning losses of a single gear gearbox are evaluated using computational fluid dynamics (CFD) implemented in Ansys. Several baffle clearances are evaluated from 39.29 mm to 114.29 mm. The gear rotates at 1307 RPM and the gearbox oil level is set at the midpoint of the gear when at rest. The metric for baffle evaluation is the energy consumed over the simulation time. To determine baffle locations with potential maximum and minimum churning energy loss, an optimization is performed using a function obtained from the fit of data extracted from the CFD results. Results show that (a) energy associated with churning loss is minimized when the baffle is either very close or very far from the gear, (b) baffle clearances that cause maximum or minimum energy consumption can be tentatively identified, (c) there are certain ranges of baffle clearances that cause less energy consumption than other ranges, and (d) effective coupling of CFD and optimization methodologies for baffle studies requires significant computational resources.

Contents

List of Tables	v
List of Figures	vi
1. Literature Review	1
1.1 Introduction	1
1.2 Background	2
1.3 Geometry	6
1.4 Lubrication	9
1.5 Baffles	12
1.5.1 Axial Baffles	13
1.5.2 Radial Baffles	15
1.6 Literature Review Summary	18
1.7 Thesis Overview	19
2. Literature Results Analysis	20
2.1 Lubrication	20
2.2 Axial Baffles	21
2.3 Radial Baffles	23
3. Gearbox Geometry	25
3.1 TGB Model	25
3.1.1 Gear Properties	25
3.1.2 Fluid Properties	27
3.1.3 Baffle Properties	27
3.2 Single Gearbox Model	28
3.2.1 Gear Properties	28
3.2.2 Oil Properties	29
3.2.3 Baffle Properties	29
4. CFD Basics	32
4.1 TGB Gear Set	32
4.1.1 Geometry	32
4.1.2 Mesh	33
4.2 Single Gear Box (SGB)	39
4.2.1 Geometry	39
4.2.2 Mesh	39

4.3 CFD Solver	40
4.3.1 Solver Type.....	40
4.3.2 Models	41
4.3.3 Boundary and Cell Zone Conditions and Movement	42
4.3.4 Solution Methods.....	44
4.4 Fidelity versus Computing Time	46
5. Simulation Results.....	48
5.1 Simulation Progression	48
5.2 Obstacles and Solutions	56
5.4 Results.....	57
6. Optimization	62
6.1 Churning Loss Optimization	62
7. Optimization Results	70
7.1 Optimum Baffle Location	70
7.2 Torque Loss Data.....	70
7.3 Energy Consumption for Oil and Air.....	72
7.4 Energy Consumption for Oil Only.....	75
8. Conclusions and Future Work	78
8.1 Conclusions	78
8.2 Future Work.....	79
8.2.1 Expand to Steady State	79
8.2.2 Expand to TGB Gearbox	80
8.2.3 Expand Optimization to Other Baffle Types	80
References	81
Appendices	84
<u>Appendix A:</u> Energy Oil and Air MATLAB File	85
<u>Appendix B:</u> Energy Oil only MATLAB File	89
<u>Appendix C:</u> Torque Oil and Air at 0.113 Seconds MATLAB Code.....	93
<u>Appendix D:</u> Torque Oil Only at 0.113 Seconds MATLAB Code	97
<u>Appendix E:</u> Parallel vs. Serial Computing	101

List of Tables

1: Literature Review Summary	18
2: Gear Dimensions	25
3: Under-Relaxation Factor Values	45
4: Under-Relaxation Values for the One Gear Simulation	45
5: Under-Relaxation Values for Rotating Cylinder	49
6: Under-Relaxation Factors for Four Tooth Gear	51
7: Under-Relaxation Factors of Pinion Gear without Axle	52
8: Under-Relaxation Factors of Driven Gear with Axle	54
9: Under-Relaxation Values for the Two Cylinder Model	54
10: Under-Relaxation Factors of Full TGB Gearbox	55
11: Air and Oil Energy Consumed	63
12: Single Gear Torque at 0.113 Seconds for Oil and Air	65
13: Single Gear Energy Consumed for Oil Only at 0.113 Seconds	67
14: Single Gear Energy Consumed by Air and Oil at 0.0759 Seconds	73
15: Single Gear Energy Consumed by Air and Oil at 0.113 Seconds	74
16: Single Gear Energy Consumed by Oil Only at 0.0759 Seconds	75
17: Energy Consumption at 0.113 Seconds for Oil Only	76

List of Figures

1: Gear Basics from [28]	3
2: Definition of Axial Clearance Between a Baffle and Gear.....	12
3: Definition of Radial Clearance Between a Baffle and Gear	13
4: Types of Radial Baffles a) Boards b) Semicircle c) Oval d) Snowman.....	16
5: Normalized Lubricant Depth. Data Extracted from References [1], [4], [35], [37], [38]	21
6: Normalized Axial Baffle Data Extracted from [8], [38]	22
7: Normalized Radial Clearance. Data Extracted from [8], and [31]	24
8: Inner Enclosure Dimensions of TGB Gearbox.....	26
9: Dexron VI Viscosity versus Temperature [39]	27
10: Single Gear Geometry	29
11: Clearance Between the Bottom of the Gearbox and the Teeth of the Gear	30
12: Baffle Clearances Between Gear Teeth and Baffle a) 114.29 mm b) 89.29 mm c) 64.29 mm d) 39.29 mm	31
13: Tooth Gap Variations [40]	32
14: Mesh Skewness Bar Graph.....	34
15: Mesh Orthogonality Bar Graph	35
16: Fine Detail Area of Mesh.....	36
17: Fine Mesh Areas of the TGB Gearbox	37
18: Prism Layers	38
19: Inflation Layers Added to Single Gear	40
20: Single Gear Interface.....	42
21: TGB Interface Boundaries	43
22: Simulation Progression	48
23: Single Rotating Gear not Touching the Enclosure (No Axle).....	49
24: Single Rotating Gear with Axle	50
25: Four Tooth Gear.....	51
26: Pinion Gear without Axle	52
27: Driven Gear with Axle	53
28: Full TGB Gearbox.....	55
29: All Fluids Torque for Each Baffle Location	58
30: Oil Only Torque for all Baffle Locations	58
31: Y Forces on Gear for Each Baffle Clearance.....	60
32: Z Forces on Gear for Each Baffle Clearance.....	60
33: X Forces on Gear for Each Baffle Clearance.....	61
34: Single Gear Energy Consumption for both Air and Oil at 0.113 Seconds.....	63
35: Optimization Algorithm Flowchart.....	64
36: Single Gear Torque for Oil and Air at 0.113 Seconds.....	66
37: Single Gear Energy Consumed at 0.113 Seconds for Oil Only.....	68
38: Volume of Fluid of Rotating Fluid with Red as Oil and Blue as Air.....	69
39: Location of Optimum Baffle	70
40: Torque Consumed Magnitude for all Baffle Clearances for Oil and Air	71
41: Torque Consumed Magnitude for all Baffle Clearances for Oil Only	72
42: Single Gear Energy Consumed at 0.0759 Seconds by Air and Oil	73

43: Energy Consumed by Air and Oil at 0.113 Seconds	74
44: Single Gear Energy Consumed by Oil Only at 0.0759 Seconds	75
45: Single Gear Energy Consumed by Oil Only at 0.113 Seconds	76

1. Literature Review

1.1 Introduction

Gear boxes are critical components in applications ranging from automobiles to airplanes. As the gears rotate, some of the mechanical energy is used to overcome frictional losses between solid surfaces (e.g. due to gear meshing) and solid-fluid interfaces (e.g., windage, lubricated bearings, and churning). Depending on the gearbox application, one or more types of losses may be relevant. In broad terms, the power loss due to churning (i.e., churning losses) is caused by the interaction of a mechanical component that is immersed in a two-phase, lubricant-air mixture Concli et al[1]. Windage losses occur due to friction between a gear rotating in air or air-lubricant mist Concli et al. [1].

For many reasons, reducing churning losses has been the focus of several investigations including Luke and Olver[2], Kolekar et al. [3], Hohn et al. [4], Andersson [5], Petry-Johnson et al. [6], Ariua et al. [7], Changenet and Vexel [8], and Arisawa et al. [9]. One such reason is that since a portion of the input power must be used to overcome friction, the gearbox mechanical efficiency is reduced. The dissipation of this frictional energy into heat may increase the lubricant temperature, potentially shortening lubricant (and gear) life. Practical impacts may include a reduction in product reliability and increases in cooling system and maintenance costs.

The goal of this chapter is to review baffle design and implementation approaches to reducing churning losses of gears in dip lubrication. Dip lubrication is when the gears are (partially or fully) submerged in a lubrication bath, whereas targeted lubrication occurs when

the gear is lubricated at specific locations using a jet. Studies on windage losses with no lubrication can be found in references [10]-[16] while targeted lubrication investigations are available in references [7] and [17]-[20] .

Although gear boxes are widely used in many industrial, medical, and aerospace applications, this review focuses on gear systems for power transfer in vehicles. Furthermore, this chapter will focus on a review of dip lubrication, for which churning losses are most relevant. Bevel gears fall outside of the scope of this review because of the literature reviewed none of the bevel gears were dip lubricated and therefore they do not undergo churning losses. Several researchers that have investigated the power losses of bevel gears include Arisawa et al. [9], Winfree [21], Johnson et al. [22] for targeted lubrication and Rapley et al. [24][25] , Lord [12], and Farral et al. [26] for no lubrication. Bearing losses and meshing losses are also outside of the scope of this review.

Churning power losses can be impacted by modifying the gear geometry, changing the lubricant level or through the implementation of baffles covering all or a portion of the gear. Finally, this review will focus mostly on the effect that baffles have on reducing churning losses but will also review other methods by which churning losses can be reduced.

1.2 Background

Several authors have investigated both analytical and empirical methods to calculate or predict churning losses. Boness [27] developed three equations for the drag moment coefficient. Each equation targets a different flow regime (i.e., laminar Eq. (1), transition Eq. (2), or turbulent Eq. (3)):

$$C_m = \frac{20}{Re} \quad (1)$$

$$C_m = (8.6 * 10^{-4}) \times Re^{\frac{1}{3}} \quad (2)$$

$$C_m = \frac{5 \times 10^8}{Re^2} \quad (3)$$

where C_m is the dimensionless drag coefficient, and Re is the Reynolds number. The drag moment coefficients are used to find the power loss according to Eq. (4):

$$M = \frac{C_m \times \frac{1}{2} \times \rho \times \omega^2 \times R^5}{2} \quad (4)$$

where M is the friction torque, ρ is the fluid density, ω is the angular velocity, and R is the pitch circle radius. The power loss is equal to the product of M and the angular velocity. The pitch circle radius of a gear can be seen in Figure 1.

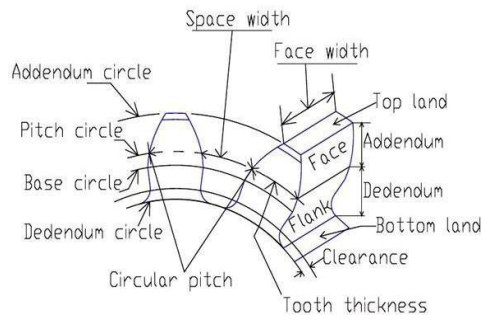


Figure 1: Gear Basics from [28]

These equations are only used to predict churning loss if the normalized lubricant depth is 0.9 or less. The normalized lubricant depth can be calculated using Eq. (5):

$$\bar{h} = \frac{h}{h_{avg}} \quad (5)$$

Terekhov [29] also found equations for the drag moment coefficient that are used to find the torque:

$$C_m = 4.57 \times Re^{-0.6} \times Fr^{-0.25} \times \left(\frac{h}{R}\right)^{1.5} \times \left(\frac{b}{R}\right)^{-0.4} \times \left(\frac{V_g}{V_o}\right)^{-0.3} \times \left(\frac{\Sigma V_g}{V_o}\right)^{-0.2} \quad (6)$$

$$C_m = 2.63 \times Re^{-0.6} \times Fr^{-0.25} \times \left(\frac{h}{R}\right)^{1.5} \times \left(\frac{b}{R}\right)^{-0.17} \times \left(\frac{V_g}{V_o}\right)^{-0.53} \times \left(\frac{\Sigma V_g}{V_o}\right)^{-0.2} \quad (7)$$

$$C_m = 0.376 \times Re^{-0.3} \times Fr^{-0.25} \times \left(\frac{h}{R}\right)^{1.5} \times \left(\frac{b}{R}\right)^{-0.124} \times \left(\frac{V_g}{V_o}\right)^{-0.376} \times \left(\frac{\Sigma V_g}{V_o}\right)^{-0.2} \quad (8)$$

$$M_{oe} = C_m \times \rho \times \omega^2 \times R^3 \times b \times l \quad (9)$$

where Fr is the Froude number, V_g is volume of the gear from the point of immersion, V_o is the volume of oil, and M_{oe} is moment of losses due to oil expulsion from the spaces between the teeth. Terekhov [29] used a different equation for the drag moment coefficient for each way that the lubricant moved around the gear changed. Eq. (6) and Eq. (7) are used when the lubricant moves around the disk in an almost laminar way, whereas Eq. (8) is used when the lubricant is thrown from the disk. Luke and Olver [2] compared equations that calculate churning torque found by both Boness and Terekhov. It was found that neither of these sets of equations were very accurate. The equations by Boness are noteworthy due to having three unique zones; laminar, transient and turbulent flows. The experimental set-up of Luke and Olver found that there was no “transient” flow section of the moment coefficient. Also, Luke and Olver found that the turbulent equation from Boness is not accurate for viscous lubricants. Terekhov’s equations are more complex than Boness but are still similar. The Terekhov equations for mating gears have modest correlation to experimental results according to Luke and Olver. More complex models incorporating the effects of viscosity, density, and surface

tension of the lubricant have been developed by several researchers. Kolekar et al. [3] investigated the effect of surface tension, temperature, starting speeds, and air pressure inside the gear housing on the churning losses. The study found that as the surface tension of the lubricant decreases, the churning loss also decreases. Also, when the air pressure inside the housing is increased the churning loss decreases. The directly proportional relationship between lubricant viscosity and churning losses was experimentally confirmed by Kolekar et al.[3], Shimokawa [30], and Chen and Matsumoto [31].

Changenet et al. [8] have also investigated churning losses. Similar to Boness [27], Changenet et al. calculated the churning torque from a dimensionless torque. That dimensionless torque is calculated in different ways based on the Reynolds number. Equation (12) shows the churning torque, and equations (10) and (11) show two different ways to calculate the dimensionless torque.

If $Re < 6000$:

$$C_m = 1.366 \times \left(\frac{h}{D_p}\right)^{0.45} \times \left(\frac{V_o}{D_p^3}\right)^{0.1} \times Fr^{-0.6} \times Re^{-0.21} \quad (10)$$

If $Re > 9000$:

$$C_m = 3.644 \times \left(\frac{h}{D_p}\right)^{0.1} \times \left(\frac{V_o}{D_p^3}\right)^{-0.35} \times Fr^{-0.88} \times \left(\frac{b}{D_p}\right)^{0.85} \quad (11)$$

$$C_{ch} = 0.5 \times \rho \times \omega^2 \times R^3 \times S_m \times C_m \quad (12)$$

where D_p is the pitch diameter, C_{ch} is the churning torque and S_m is the immersed surface area.

Further, computational fluid dynamics (CFD) has been used to model and predict churning losses. Gorla et al. [15] created a CFD model of a single gear in a gearbox fully immersed in

lubricant, to determine if CFD could accurately predict splashing (churning) power losses. The CFD model was experimentally validated, achieving an error of less than 5% [15]. One of the possible reasons for the discrepancy is that the CFD model used constant temperature values while in the experimental data the temperature varied [15]. This caused a discrepancy because the temperature affects the viscosity of the lubricant, which in turn can affect the churning power losses. Kraetschmer et al. [33] also developed a CFD model of a gear pair to estimate splash power losses (both churning and windage). The model was experimentally validated to estimate the churning and windage losses of a gear pair. There were some advantages of CFD according to Kraetschmer et al. [33]: CFD has a lower cost than experimental work and can model the dynamic lubrication level and the direction of rotation, whereas empirical and analytical models cannot.

1.3 Geometry

The effect of gear geometry on churning losses stem from how the lubricant is displaced by the gear. A gear that has a larger volume displaces more lubricant than a gear with a smaller volume. Concli et al. [1], Seetharaman et al. [34], [35], and Desai [36] have investigated the effect of gear geometry, specifically face width and modulus, on churning losses.

Concli et al. [1] first defined the different types of power losses, including churning, and determined how to calculate these losses. A CFD model of a single gear with FVA2 oil was used for this research. Concli's defined torque as

$$T = \Sigma (v_{mix} \times \rho_{mix} \times \frac{\delta U}{\delta x}) \times A \times r \quad (13)$$

$$\tau = (v_{mix} \times \rho_{mix} \times \frac{\delta U}{\delta x}) \quad (14)$$

where τ is the shear stress of a cell in the CFD model while A is the area of a cell and r is the radial distance from the cell to the gear axis. Once the losses were defined, Concli developed a CFD model to test different factors of churning losses in a parametric study. The study focused on investigating the influence of gear tip diameter and face width on the churning torque. Gear tip diameter is defined as the diameter of the gear at the tip of the tooth. It was found that increasing the gear tip diameter (from 96.5 mm to 102.5 mm in this study) increased the churning torque, although the magnitude of the increase in the churning torque was also dependent on the speed of the gear. As the gear speed was increased the rate of growth of the churning torque also increased. It was found in this study that increasing the face width (from 20 mm to 40 mm) would increase the churning torque. The gear speed also played a role in how the churning torque increased. When the gear has a speed of 8000 RPM a decrease in face width from 40 mm to 20 mm results in a 44% churning torque reduction, while only a 40% reduction of churning torque occurred when the gear was at 5000 RPM. Because churning power losses decrease as churning torque decreases, Concli et al. determined that churning torque increased as the face width or tip diameter increased. This is most likely due to the increase in the lever arm.

Seetharaman et al. [34][35] experimentally investigated the effect of module, face width, lubricant depth, and rotational direction. The base gear had a module of 2.32 mm, a face width of 19.5 mm, and oil level of 50%. For each test, one of the aforementioned factors was changed while the rest were held constant. The speed of the gear was varied to provide sufficient data points. The test rig of the experiment was kept the same, as well as the

orientation of the gears. In the study, spin losses are defined as the combination of churning and windage losses. As the gear module was changed from 2.32 mm to 3.95 mm, spin power losses were found to change from 0.78kW to 0.7kW, a change of around 11%, suggesting that gear module has a small if not negligible effect on the total spin power loss. In the same study, three face widths (14.7 mm, 19.5 mm, and 26.7mm) were tested to determine the effect of face width on total spin power loss. Results showed that total spin losses increase with face width increase and that the effect is also rotational speed dependent. For example, at the conditions tested, at 4000 RPM, the face width reduction from 26.7 mm to 19.5 mm caused a 35% total spin power loss reduction, whereas a 26.7 mm to 14.7 mm face width reduction led to a 50% reduction in total spin power losses. The same reduction in face width of 26.7 mm to 14.7 mm at 3000 RPM led to a 45% reduction in total spin power losses. This rise in total spin losses became more noticeable with an increase in the gear face width or rotational speed.

Desai [36] created a model of planetary gears to test the effect of module and face width on total spin power loss, including power loss due to churning. The planetary gear set used by Desai consisted of spur gears used as ring gears, planet gears, and a sun gear. During the experiment Desai changed the gear module, and the gear face width. The original module of 2.5 mm was reduced to 1.9 mm, and then increased to 2 mm. It was found that the churning power loss was not significantly affected by the module (a finding similar to Seetharaman et al. [34][35]). Desai also observed the effect of face width on the churning losses. Two experimental set-ups were used to test the effect of face width on churning power loss. The first reduced the planetary gear face width while the sun gear face width was held constant.

The second set-up increased the planetary face width while reducing the sun face width. Large changes in churning power losses were observed between the two set-ups.

Churning power losses can be affected by the geometry of the gear. If the tip diameter of the gear increases or the face width of the gear increases, then the churning loss will also increase. The rate of this increase in churning loss is determined by the speed of the gear, the higher the speed the larger the rate. One part of the gear geometry that doesn't have a large impact on the churning power loss of gears is the module. Studies suggest that a change in the module will not significantly change in the churning loss.

1.4 Lubrication

Churning losses are caused by gear and lubricant interaction. This interaction is affected by the amount of lubricant in the gear box which along with the system geometry, determines the lubrication level. Studies on the relationship between lubrication level and churning losses include Concli et al. [1], Seetharaman et al. [34][35], Michaelis et al. [4][37], and Polly [38].

Concli et al. [1] developed a model to determine the churning losses of a spur gear pair as face width, lubricant level, and tip diameter were varied. In this simulation FVA2 lubricant was used, and the original case had a face width of 40 mm, lubricant level of 50%, and module of 4 mm, and tip diameter of 102.5 mm. During this experiment the effect of the change of each factor was tested individually. Lubrication level is typically defined in terms of percent coverage of the gear surface area. This study targeted 100%, 50%, and 25% coverage. When the lubrication level was reduced from 100% to 50%, the churning torque was reduced by 60%. It was also found that when the lubricant level was 25% the churning torque was only 30% of

the churning torque of the 50% lubrication. These percentage of reductions occurred at all gear speeds. Overall Concli et al. results suggest a direct (and significant) relationship between churning losses and lubricant level.

Seetharaman et al. [34][35] created a physics-based model to help predict churning power loss and then performed experimental testing. The lubricant level's effect on churning power loss was found in both the simulation and the experiment as

$$P_{dp} = 4\mu br_o^2 \omega^2 \times \cos^{-1}[1 - \bar{h}] \quad (15)$$

where P_{dp} is the periphery drag power loss, μ is the viscosity, b is the tooth face width, r_o is the outside radius, ω is the angular velocity, and h is the lubricant depth. At 75%, 50%, 25%, and 2.5% coverage. From both the prediction and the experiment, it was found that as the lubricant level was decreased, the churning power loss was reduced. At 4000 RPM, the reduction was 30% from 75% coverage to 50% coverage whereas the reduction was 80% from 75% coverage to 2.5% coverage. The amount of reduction in churning power loss was also affected by the speed of the gears. At 3000 RPM the percent reduction in churning power loss was 20% when the lubrication level was reduced from 75% coverage to 50% coverage, instead of the 30% churning power loss reduction at 4000 RPM. As the gear speed increased larger reductions of churning power losses were observed.

Michaelis et al. [4][37] tested a two-gear gear box to determine what factors affected the no-load power loss. No load power losses consist of losses from the effect of lubricant interacting with the bearing (bearing losses) and lubricant interacting with the gear (churning losses). One of the factors that was tested by Michaelis et al. [37] was lubrication depth. The

different levels of lubricant were at the center line, at three times the module of the pinion, at three times the module of the gear and at one times the module of the gear. These levels translated to 50%, 29.8%, 11.2% and 3.6% coverage, respectively. It was determined that as the level of lubricant was decreased, the no-load torque loss was decreased. This pattern occurred until the lubricant level was reduced to one times the module of the gear, in this case the no-load torque loss either didn't change from the value at three times the module gear or it increased depending on the speed of the gear. It was also determined that when the lubricant level was decreased from the center line to three times the module of the gear the no-load torque loss was reduced by more than 50% for all speeds.

Polly [38] explored the effects of the lubrication level on spin power loss using a twin gear set-up. Lubrication level was tested at 100%, 75%, 50%, 37.5%, 25%, 12.5%, and 2.5% coverage. The spin power losses decreased almost linearly. At 2000 RPM, a decrease from 100% coverage to 2.5% coverage resulted in a power loss reduction of over 90% during experiments. It was also found that the slope of the line depicting the relationship between the lubricant level and spin power losses increased as the speed of the gears increased. At 1000 RPM a decrease in coverage from 100% to 2.5% only has a reduction of 85% possible. When examining differences between gear blanks, spur gears and helical gears, it was discovered by Polly [38] that, for most speeds and most lubricant levels, gear blanks have lower power losses than helical gears, which have lower power losses than spur gears.

In summary, past work indicates that as the lubricant level decreases, the power losses also decrease. Results presented here show the same general pattern regardless of the different geometries used by each researcher.

1.5 Baffles

Various studies have shown that shrouding gears in dip lubrication can significantly reduce churning losses in gear boxes [8], [30], [31], [38]. Both axial and radial baffles have been investigated. Axial baffles are shapes that are placed certain distances (axially) from the face of the gears to constrain lubricant motion perpendicular to the gear axis, seen in Figure 2.

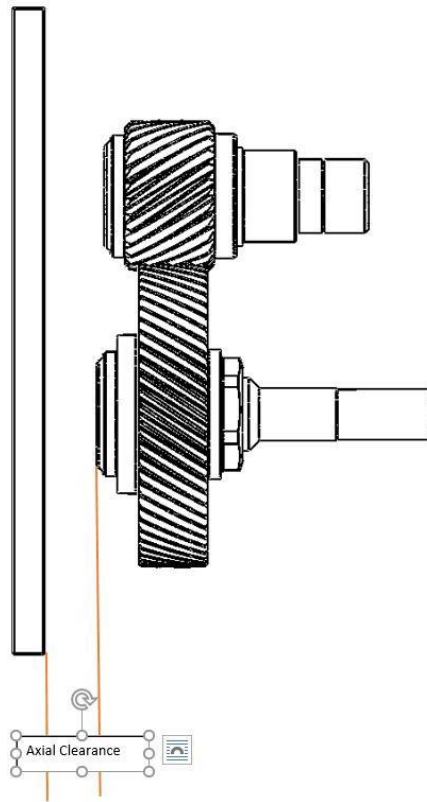


Figure 2: Definition of Axial Clearance Between a Baffle and Gear

Radial baffles are shapes that are placed at radial distances from the gear teeth, to constrain lubricant flow around the teeth, seen in Figure 3.

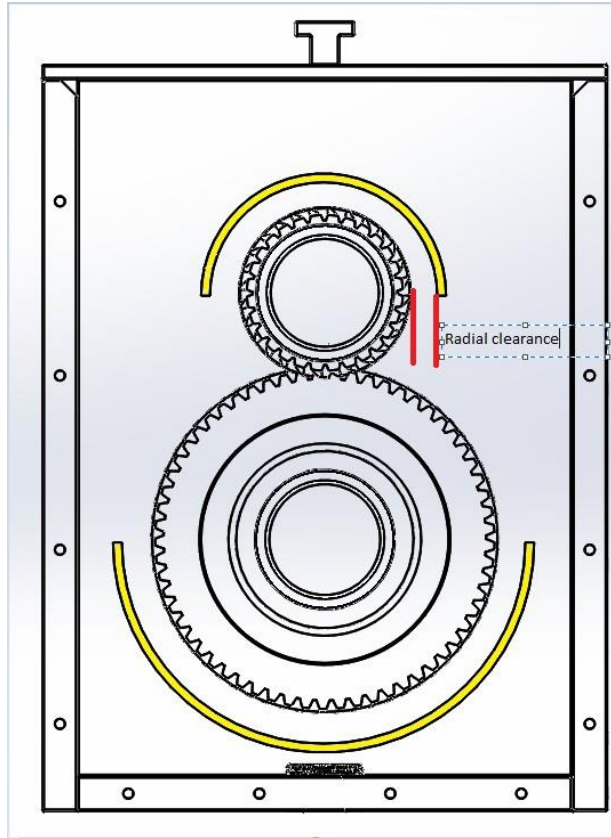


Figure 3: Definition of Radial Clearance Between a Baffle and Gear

1.5.1 Axial Baffles

Baffles affect churning losses by changing how the lubricant interacts with the gear. An axial baffle will accomplish this by limiting the flow around the face of the gear, whether the gear is spur or helical. Several researchers have observed the effect an axial baffle will have on a gear box including Shimokawa [30], Changenet and Vexex [8], and Polly [38].

Shimokawa [30] explored ways to improve the Jatco CVT8 transmission. To accomplish this Shimokawa reduced the lubricant level and added an axial baffle. When the axial baffle was added to the CVT8, the effect of the clearance between the baffle and gear face was not considered. Instead, the effect of the extent of the area covered by the baffle was explored. In

the investigation, the area of the gear face covered by the baffle was varied. It was discovered that if the lubricant level was high, baffles that covered less of the gear face caused lower mechanical loss. As the lubricant level was decreased, baffles became more effective as the area of gear covered was increased.

Changenet and Velex [8] built a gear box to test how baffles affect churning losses. The axial baffle that this test configuration used had clearances that varied from 1 mm-10 mm. Changenet and Velex ran the test box with various axial clearances to determine the reduction of power losses. A churning power loss reduction of up to 50% was found at 1000 RPM and at 2000 RPM when the axial clearance was decreased from 10 mm to 1 mm. The axial clearance was not the only factor that Changenet and Velex investigated: whether two axial baffles were needed or if a single axial baffle would suffice was also explored. Changenet and Velex concluded that if there are axial baffles on each side of the gear, then the smallest clearance is the clearance that dictates the size of reduction in power losses. A gear with an axial clearance of 1 mm on one side and 10 mm on the other would have similar power loss as those of a gear that had two axial baffles of 1 mm clearance.

Polly [38] created a gearbox to help determine different factors that affect power loss, including axial clearance. Polly investigated the effect of these clearances between 1 mm and 12 mm by holding other factors such as radial clearance and lubricant level constant while the axial clearance was decreased. This experiment was done at multiple gear speeds and multiple lubricant levels. The overall pattern was that as the axial clearances were decreased the spin power losses also decreased. The extent of the decrease was affected by the speed of the gear and the lubricant level. A decrease in axial clearance from 12 mm to 1 mm caused a decrease

in spin losses over 50%. At lubricant levels above the center line, the decrease in power loss is larger as the axial clearance decreases from 12 to 1 mm. At lubricant levels below the center line the decrease in power loss is less significant.

1.5.2 Radial Baffles

Axial baffles are not the only type of baffle that can influence churning losses. A radial baffle can also reduce the churning power loss of a gear set. Each type of the baffle may affect churning losses differently. Several researchers have observed the difference in effect between axial and radial baffles [8] [31][38].

Unlike axial baffles (which cover the face of the gear), radial baffles have been investigated with several different shapes as seen in Figure 4. The shape of the radial baffle affects the reduction of churning losses.

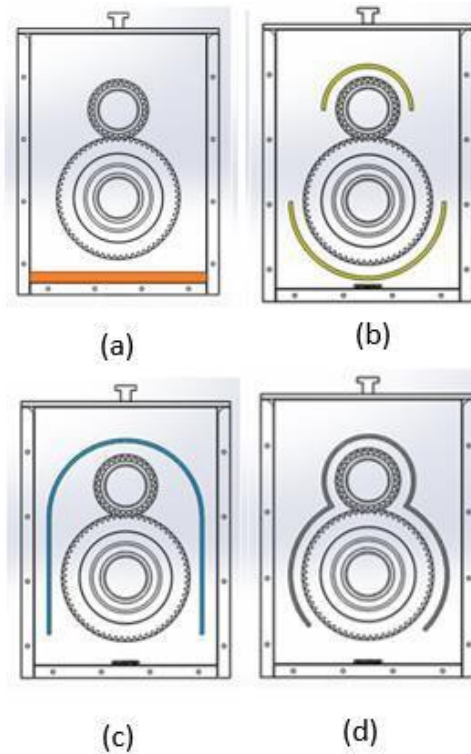


Figure 4: Types of Radial Baffles a) Boards b) Semicircle c) Oval d) Snowman

Chen and Matsumoto [31] created an experimental rig that would allow for the shape of the radial baffle, the clearance of the radial baffle, as well as several other factors that could influence the churning loss to change. The shapes of radial baffles used in the test rig were the snowman, the oval and the boards as seen in Figure 4. For all three shapes, the clearance was also changed from 7 mm to 17 mm. From this experiment they found that if a snowman or oval radial baffle with a clearance of 7 mm was used, then there would be an increase in churning losses up to 300% compared to the un baffled gearset. This leads to the conclusion that, for this configuration, there is a minimum radial clearance for certain shapes of radial baffles that when violated results in increased churning losses. It was also found that for the boards at 7 mm, and the boards, oval, and snowman at 17 mm clearance, the churning loss was reduced compared to the no baffle churning loss. The 7 mm boards had a churning power loss reduction up to

66%. When the radial clearance was 17 mm, the boards shaped baffle led to a power loss reduction of up to 66%, the oval shape caused a reduction of up to 33%, and the snowman reduced churning power by up to 44%. It was found that the most effective radial baffle to reduce churning losses was the boards, as both clearances for the boards caused close to 66% power loss reduction (PLR).

Changenet and Velez [8] built an experimental test set up to explore the effect of both axial and radial baffles on the reduction of churning losses. The radial clearances used were 5 mm and 10 mm. It was observed that as the radial clearance was increased the reduction in losses decreased. The magnitude of the reduction caused by the increase in radial clearance was affected by the speed of the gear, and the axial clearance if there was an axial baffle. The largest reduction in power losses that was observed was 11% at 4000 RPM, with constant 7 mm axial clearance and an increase of radial clearance from 5 mm to 10 mm. At smaller axial clearances and at higher speeds, the change in radial clearance had less effect.

Polly's [38] test rig was built for experiments that changed the radial clearances of baffles between 5 mm and 12 mm. Results showed that for lower lubricant depths, the 5 mm radial clearance had the lower spin power losses, but for the lubricant levels that were at or above the center line of the gear, the 12 mm clearance had the lower spin power loss. The difference in the spin power losses between 5 mm and 12 mm clearance were not large and varied not only by lubricant level but also by speed of the gear. The largest reduction in power loss caused by reducing the radial clearance was 10%. All these factors suggest that the radial baffle is not as effective at reducing the spin power loss (PL) as the axial baffle.

1.6 Literature Review Summary

This review described several studies that have investigated churning losses in dip lubrication. These past investigations showed that gear geometry, specifically face width, lubrication level and both axial and radial baffles have varying effect on the reduction of churning losses in the gear box. Generally, it was found that as face width decreases so do churning losses. Also, as the lubricant level decreases the churning losses decrease, although this does not consider the effects of greater temperatures or increasing gear wear due to the lower fluid levels. Axial baffles decrease power loss as the clearance decreases. The amount of this reduction is larger than that of radial baffles. Although radial baffles can reduce the churning power loss, their impact is more system-specific than that of axial baffles.

Most of the investigations used unique experimental methodologies or modeled the gear and baffle system using CFD. The normalized data for the lubricant level, axial clearance, and radial clearance allow for general trends in churning losses to be found. Even with the general trends uncovered through this literature review, the specific effect of these factors on reducing churning losses is not clear, due to the unique elements of each investigation.

Table 1: Literature Review Summary

Reference	Cause of Churning Power decrease					
	Face Width Decreases	Gear Tip Diameter Decreases	Modulus Increases (almost negligent)	Lubricant Level Decreases	Decrease Axial Baffle Clearance	Decrease Radial Baffle Clearance
Concli et al. [1]	P	P		P		
Seetharaman et al. [35-36]	P		P	P		
Desai [37]	P		P			
Michaelis et al. [4] [38]				P		
Polly [39]				P	P	P (dependant on lubricant level)
Changenet and Vexex [32]					P	
Chen and Matsumoto [31]						P (dependant on baffle shape)

1.7 Thesis Overview

Current literature reveals that there is limited consensus of where to place baffles in a gearbox to minimize oil churning losses. To address this knowledge gap, an investigation of the coupling of CFD with optimization is performed to determine the placement of radial baffles that minimizes churning losses. The ultimate goal is to create a gearbox model that balances fidelity and computing time, so that the baffle location can be optimized to minimize churning losses in the gearbox. From the limited literature available, nondimensionalized baffle clearance data is presented to define currently publicly available findings. Since optimization projects are time consuming, the groundwork for the twin gear gearbox model (the TGB model) was created, but the optimization of baffle location will be performed on a single gear version of the TGB gearbox. The single gear version of the twin gearset only includes the pinion gear. CFD simulation results are used to find the optimum radial clearance to minimize the churning losses.

Chapter 2 presents the non-dimensional baffle clearance data. Chapter 3 discusses the properties of the TGB gearbox and the single gear gearbox. Chapter 4 describes the basics of CFD modeling and the creation of the TGB and single gear gearbox (SGB) simulations. Chapter 5 discusses the results of the simulations. Chapter 6 sets up the optimization study. Chapter 7 presents the results of the optimization study. Chapter 8 will present conclusions and possibilities of future work.

2.

Literature Results Analysis

2.1 Lubrication

The objectives of this chapter are to 1) quantify the effect of baffles on churning loss reduction in spur and helical gears, 2) synthesize the published technical data found in the literature review to quantify these effects, and 3) use these findings to offer perspective on the focus of further research. The literature review uncovered general patterns for the effect of lubrication on churning loss. One way to generalize the effect of how lubricant level affects the power loss of a gear pair is to normalize the researchers' results. The normalization used is

$$\bar{P}_h = \frac{P_h}{P_{h,avg}} \quad (16)$$

where P_h stands for the power loss at the tested depth, and $\bar{P}_{h,avg}$ is the power loss when the fluid depth is 50% of the pitch diameter. The depth of the gears also had to be normalized:

$$\bar{h} = \frac{h}{h_{avg}} \quad (17)$$

where h is the lubricant depth and h_{avg} is a depth of 50% of the pitch diameter. The rationale for using the 50% level of lubrication as a normalization metric is that not every researcher performed tests with a coverage of 100%, but most studies reported results at a lubricant level of 50%. The normalized data can be seen in Figure 5.

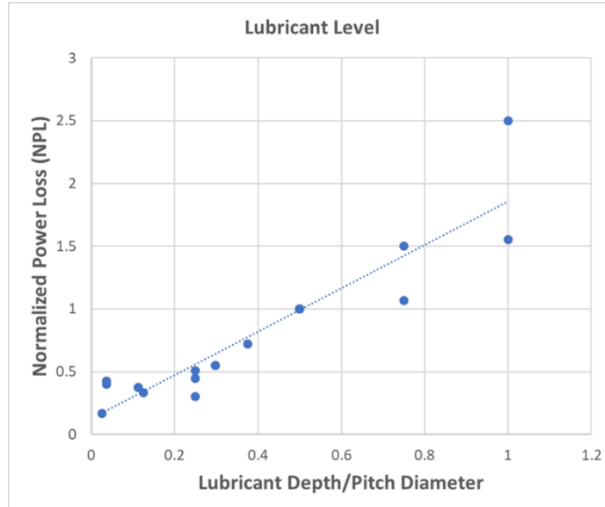


Figure 5: Normalized Lubricant Depth. Data Extracted from References [1], [4], [35], [37], [38]

As shown in Figure 5, created from data from [1] [4] [35] [37] [38], as the normalized lubricant depth decreased the normalized power loss also decreased. For the lower lubricant depths, the results were more clustered and as the lubricant depth increased toward 100%, the data were more scattered. Reductions in the lubricant level can lead to the normalized power loss decreasing by more than 50%.

2.2 Axial Baffles

It was found from the literature review that not all reported effects of axial baffles on churning power losses used the same set of gears. Therefore, the exact clearance of the axial baffle that gives the largest reduction of churning power loss cannot be determined solely from the clearance. The size of the gear must also be taken into consideration. Rather, this is accomplished by normalizing the data from Polly [38] and Changenet and Velex [8] using

$$\bar{p}_a = \frac{P_{la}}{P_{n,a}} \quad (18)$$

$$\bar{C}_a = \frac{C_a}{R} \quad (19)$$

Eq. (18) defines the normalized power loss with an axial baffle, where $P_{b,a}$ is the power loss with an axial baffle, and $P_{n,a}$ is the power loss of the gearbox without a baffle. Eq. (19) calculates the normalized axial clearance. In Eq. (19) C_a is the axial clearance and R is the pitch radius. Define the y axis clearly before discussing results. It is plotted as a power loss reduction even though the prior equations quantify power loss.

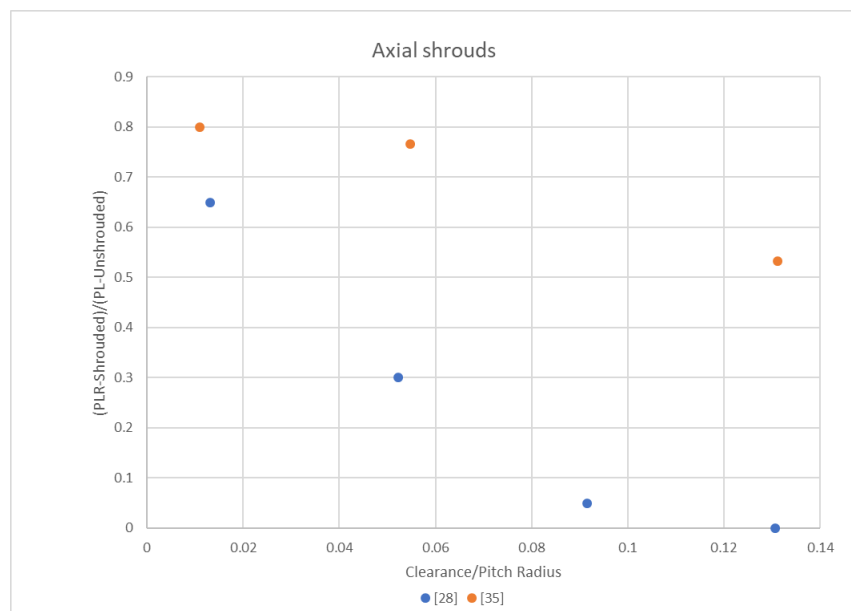


Figure 6: Normalized Axial Baffle Data Extracted from [8], [38]

In the normalized graph of Figure 6 it can be seen that as the normalized clearance is decreased the reduction in normalized churning losses increases. For the Polly [38] data (orange) it can be seen that the rate of decrease in reduction of churning losses as the clearance/pitch ratio increases is not as large as for the Changenet and Valex [8] data (blue). When the normalized axial clearance is the same for the both sets of data, the reduction in churning losses is not the same. This shows that the clearance and the pitch radius are not the

only factors that affect the churning loss. The values could also be caused by other differences in geometry of the gear or the baffle or even the lubricant level. The overall trend of both data sets is that for smaller normalized axial clearances there is a larger reduction in normalized churning losses. This means that a smaller axial clearance will cause a larger reduction in churning losses.

2.3 Radial Baffles

The researchers that have observed the effects of radial baffles on churning power losses did not all use the same set of gears or the same type of radial baffle. Therefore, the exact clearance of the radial baffle that gives the largest reduction of churning power loss cannot be determined solely from the clearance; the size of the gear must also be taken into consideration. To do this, the data from Chen et al. [31] and Changenet et al. [8] were normalized with

$$\bar{P}_r = \frac{P_{br}}{P_{n,r}} \quad (20)$$

$$C_r^- = \frac{C_r}{R} \quad (21)$$

In Eq. (20) the normalized power loss reduction was calculated. In Eq. (20) $P_{b,r}$ stands for the power loss reduction with a radial baffle and $P_{n,r}$ stands for the power loss without the baffle. Eq. (21) calculates the normalized radial clearance, where C_r stands for radial clearance and R is the pitch radius.

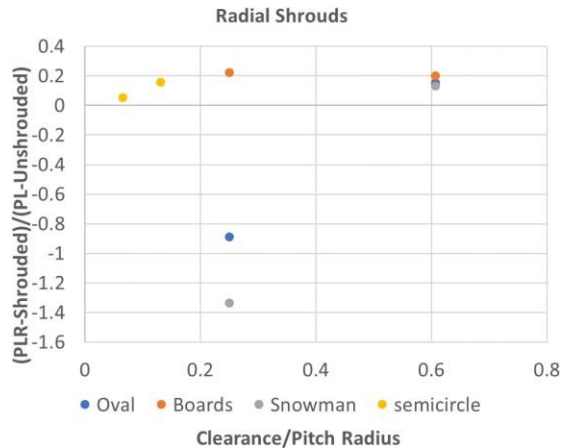


Figure 7: Normalized Radial Clearance. Data Extracted from [8], and [31]

In Figure 7, the data are arranged into sets based on the type of radial baffle. For the oval and snowman baffle shapes, the normalized power loss reduction is negative at specific normalized radial clearance, which shows that at those normalized radial clearance values the power loss increases. This means that for the snowman and oval baffles there is a point when a decrease in normalized radial clearance will cause an increase in power loss, although the specific clearance value where this occurs was not calculated. The minimum normalized radial clearance was not calculated for this paper. Due to lack of data points an accurate estimation was not possible. For the semicircle baffle, as the normalized radial clearance value decreases the reduction also decreases, so for the semicircle baffle the smallest baffle clearance does not yield the highest reduction. For the boards baffle the normalized power loss reduction is almost constant and doesn't appear to be significantly depend on the normalized clearance. The normalized data show that for radial clearances the effect on churning power loss is much more system specific than for either axial clearance or lubrication level. The effect of the radial baffle is also dependent on the type of radial baffle used.

3. Gearbox Geometry

3.1 TGB Model

3.1.1 Gear Properties

A previous project sponsored by Western Michigan University’s Center for Advanced Vehicle Design and Simulation (CAViDS) developed a high-fidelity twin gear model in Star CCM+ computational fluid dynamics (CFD) software. In the TGB gearbox, there is a driving gear and a pinion gear where both are common helical gears. The TGB model developed in this work has the same geometry as the aforementioned high-fidelity model [39].

The TGB gear set, shown in Figure 8, is enclosed in a gearbox that has the inner dimensions of 170 mm x 240 mm x 98 mm. Each wall of this enclosure is about 11 mm thick. The twin gears are centered along the 170 mm wall. The center of the driving gear is 85 mm from the bottom of the 240 mm wall. Table 2 summarizes the dimensions of the driving and pinion gears.

Table 2: Gear Dimensions

Gear	Outer Radius	Inner Radius	Addendum	Pitch Circle Radius	Helical Angle	Face Width	Tooth Thickness
Driving	59.3 mm	55.4 mm	2 mm	57.4 mm	123.5 deg	29.6 mm	3 mm
Pinion	29 mm	24.9 mm	2 mm	27 mm	123.5 deg	36 mm	3.4 mm

The gear speeds used in the present simulation are 1307 RPM for the pinion gear and - 600 RPM for the driving gear. These speeds match those used with the high-fidelity twin gear set model. By matching geometry and running conditions, to those of the high-fidelity twin gearbox model, the simulations results obtained are more easily verified.

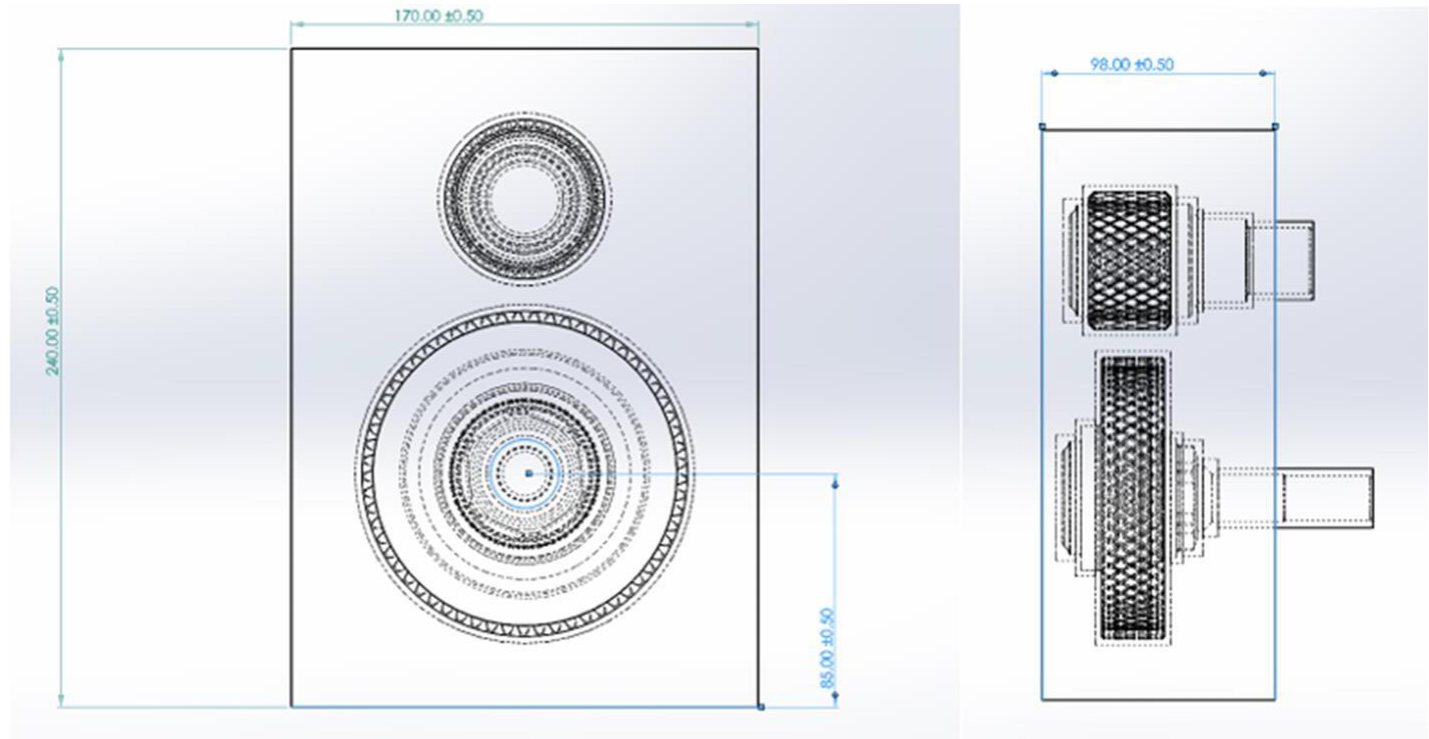


Figure 8: Inner Enclosure Dimensions of TGB Gearbox

3.1.2 Fluid Properties

The oil used is Dexron VI. For a computer simulation both the viscosity and the density of the oil need to be known at the chosen temperature. The relationship between viscosity and temperature of Dexron VI is plotted in Figure 9.

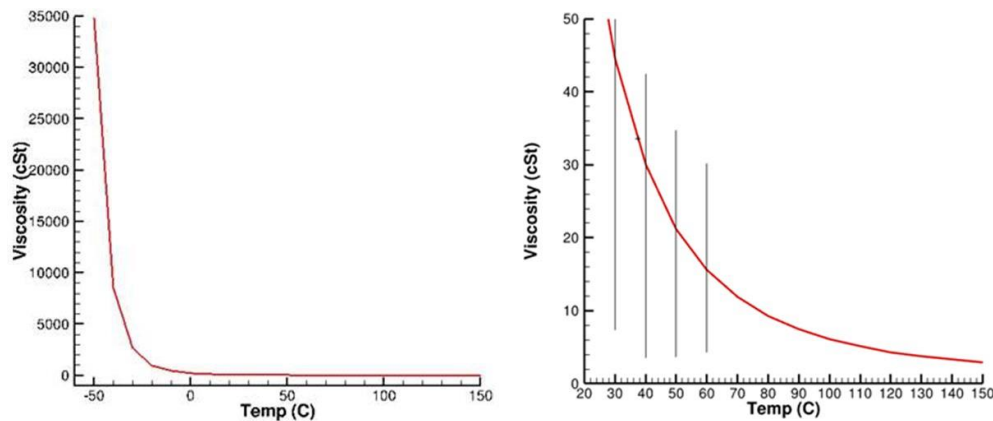


Figure 9: Dexron VI Viscosity versus Temperature [39]

The temperature chosen for the simulations was 52.5° C, to match that used with the high-fidelity twin gearbox model. At this temperature the viscosity of Dexron VI is 19.8 cSt. The density of the oil is 849 kg/m³ at 16.6° C, and 808 kg/m³ at 87° C. These values were linearly interpolated to find the density of Dexron VI at 52.5°C as 828kg/m³.

3.1.3 Baffle Properties

During the literature review, discussed in section 1.5.2, four main baffle geometries were presented: board, semi-circle, oval and snowman. The board baffle was chosen for the present investigation based on its effectiveness in reducing churning power loss. Another reason that the board baffle design was used was the simplicity of the design, which allowed for

the simulation to be run with a coarser mesh compared to the other baffle geometries, resulting in a shorter computing time.

During the literature review a graph of normalized data was created to compare results of radial baffle effect on churning power loss (Figure 7). It can be seen from Figure 7 that the board baffles are more effective at reducing power losses compared to the other three baffle types and relatively easy to implement in a twin gear setup. Both factors were reasons that board baffles were chosen for this baffle clearance optimization study. It can be seen in Figure 7 that for the board baffle, power loss reduction data are shown for values between 0.25 and 0.6 clearance/pitch radius. For the TGB gearbox used in this study, the clearances corresponding to those values are 14.35 mm and 34.44 mm. For the TGB gearbox there is only about 25 mm clearance between the bottom of the enclosure and the bottom of the driving gear.

3.2 Single Gearbox Model

3.2.1 Gear Properties

In consideration of potential long simulation times for the TGB gearbox, a simplified gearbox consisting of a single gear was also developed. The twin gear model from the previous CAViDS project was reduced to a single gear. This was accomplished by removing the larger gear from the gearbox. Figure 10 shows the single gear gearbox used in the present work. The model of it will be called the SGB (single gearbox) model.

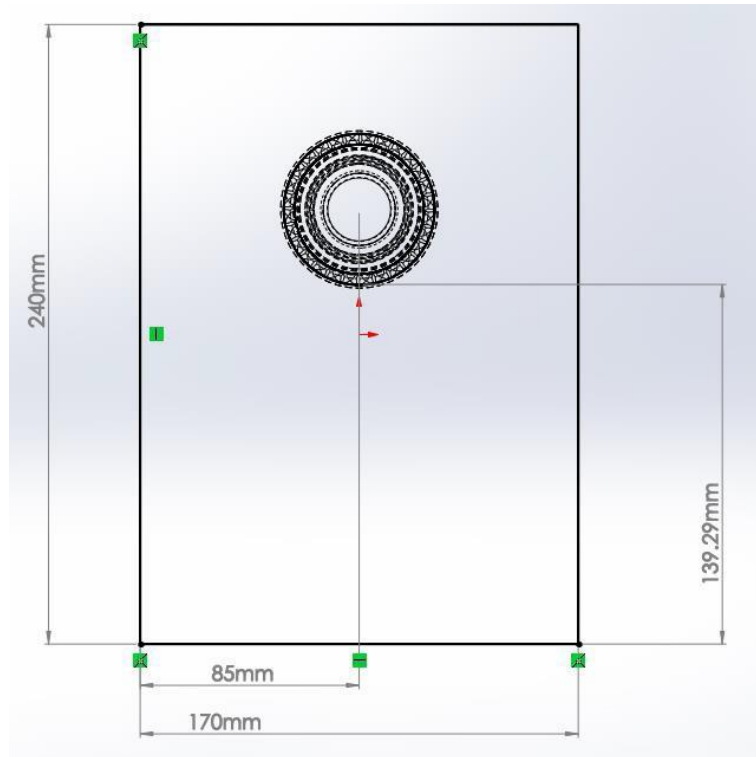


Figure 10: Single Gear Geometry

3.2.2 Oil Properties

For the single gearbox model the oil Dexron V is used at the same temperature, viscosity and density mentioned in Chapter 3.1.2. The oil level used for the single gear simulation is fixed at the midpoint of the gear face. The remainder of the enclosure space is filled with air.

3.2.3 Baffle Properties

For the single gear gearbox there is 139.29 mm clearance between the bottom of the enclosure and the bottom of the pinion gear, as seen in Figure 11. For this optimization study there will be baffles with a distance of 25 mm, 50 mm, 75 mm, and 100 mm between the bottom of the gearbox and the top of the baffle. These baffles correspond to the clearances between the baffle and the gear teeth of 114.29 mm, 89.29 mm, 64.29 mm, 39.29 mm

respectively. These clearances correspond to 4.23, 3.3, 2.38, and 1.455 clearance to pitch radius on the normalized data. The baffles can be seen in Figure 12.

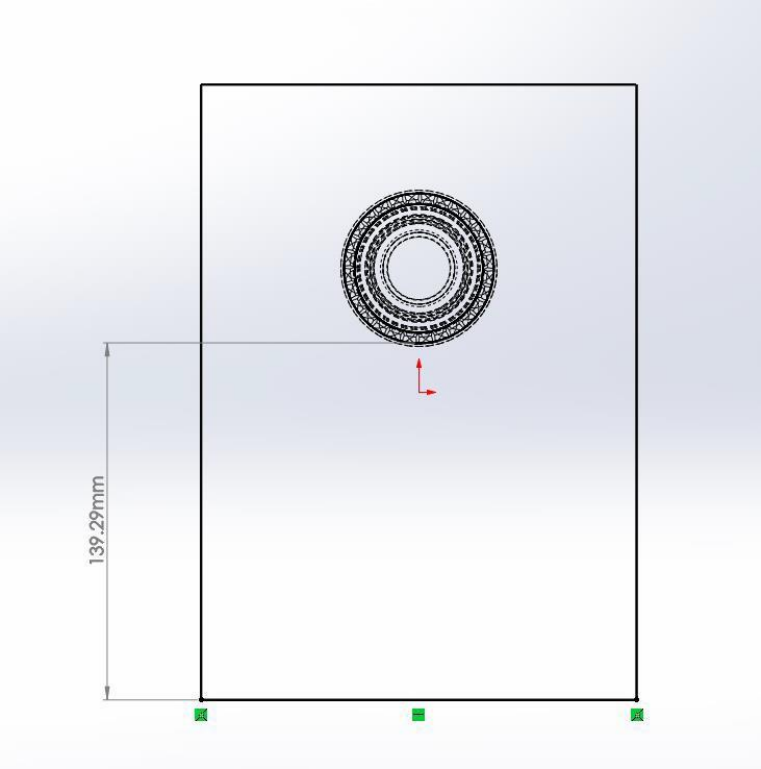


Figure 11: Clearance Between the Bottom of the Gearbox and the Teeth of the Gear

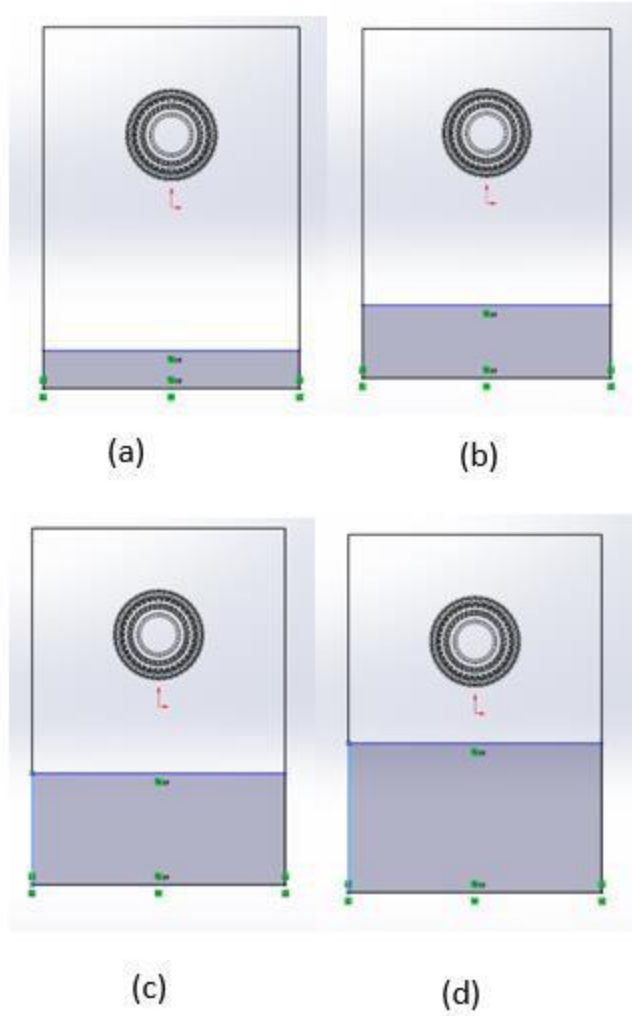


Figure 12: Baffle Clearances Between Gear Teeth and Baffle a) 114.29 mm b) 89.29 mm c) 64.29 mm d) 39.29 mm

4. CFD Basics

4.1 TGB Gear Set

4.1.1 Geometry

The gearbox geometry was created to be a simplified version of a physical twin gear setup. The gearbox was created in SolidWorks and then modified for the present work. One such adjustment is the size of the gap between the teeth of the two gears. The size of this gap was increased so that the teeth of the gear were not actually intermeshed. This allowed the simulation to focus solely on churning losses and exclude the power losses caused by physical contact between the gears. In a previous study by Yang and Liou [40] the size of the gap was varied between 13.25 mm and intermeshed. Figure 13 shows these configurations. The largest gap of 13.25 mm was utilized to study the effect of baffle clearance on power losses.

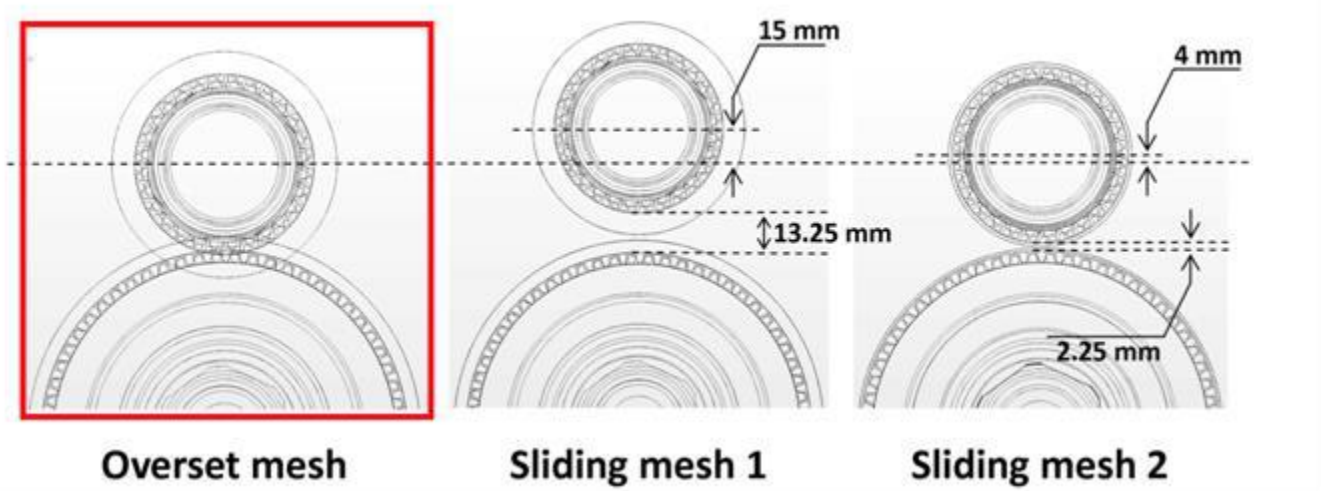


Figure 13: Tooth Gap Variations [40]

The larger gap was selected to reduce simulation time. When a mesh is created for a simulation, the finer the mesh is, the longer the simulation time required. Optimization studies

like the one to be presented shortly can be time consuming, so reducing simulation time is an important facet to consider. With a larger gap, a coarser mesh can be used without significantly compromising quality of the mesh.

4.1.2 Mesh

One of the most important aspects of a simulation is mesh creation. If the mesh is not properly constructed, the simulation can return incomplete or incorrect data. Some important considerations when constructing a mesh are skewness and orthogonal quality. Skewness is a measure of how close to ideal a mesh cell or face is. The ideal for a mesh face is an equilateral triangle for tetrahedrons and equiangular quads for quadrilaterals [41]. The use of tetras (tetrahedrons) or quads (quadrilaterals) is determined by the geometry that is meshed. Due to the irregular shape of the gears, a tetrahedral mesh is used for the baffle optimization study. Orthogonal quality is defined as the minimum value of two normalized dot product equations. The first equation is between the area vector of a face and a vector from the centroid of the cell to the centroid of that face. The second equation is between the area vector of a face and a vector from the centroid of the cell to the centroid of the next cell that shares the face [42]. Skewness and orthogonal quality are measured on a scale from 0 to 1. Skewness is generally considered of good quality if the values are below 0.9, while the orthogonal quality is considered good if the value is above 0.1. Skewness can be reduced using a finer mesh or having larger gaps between surfaces. Reducing skewness was one of the reasons for using a larger gap between the teeth of the twin gears. The skewness of the mesh can be seen in Figure 14 and the orthogonal quality of the mesh can be seen in Figure 15.

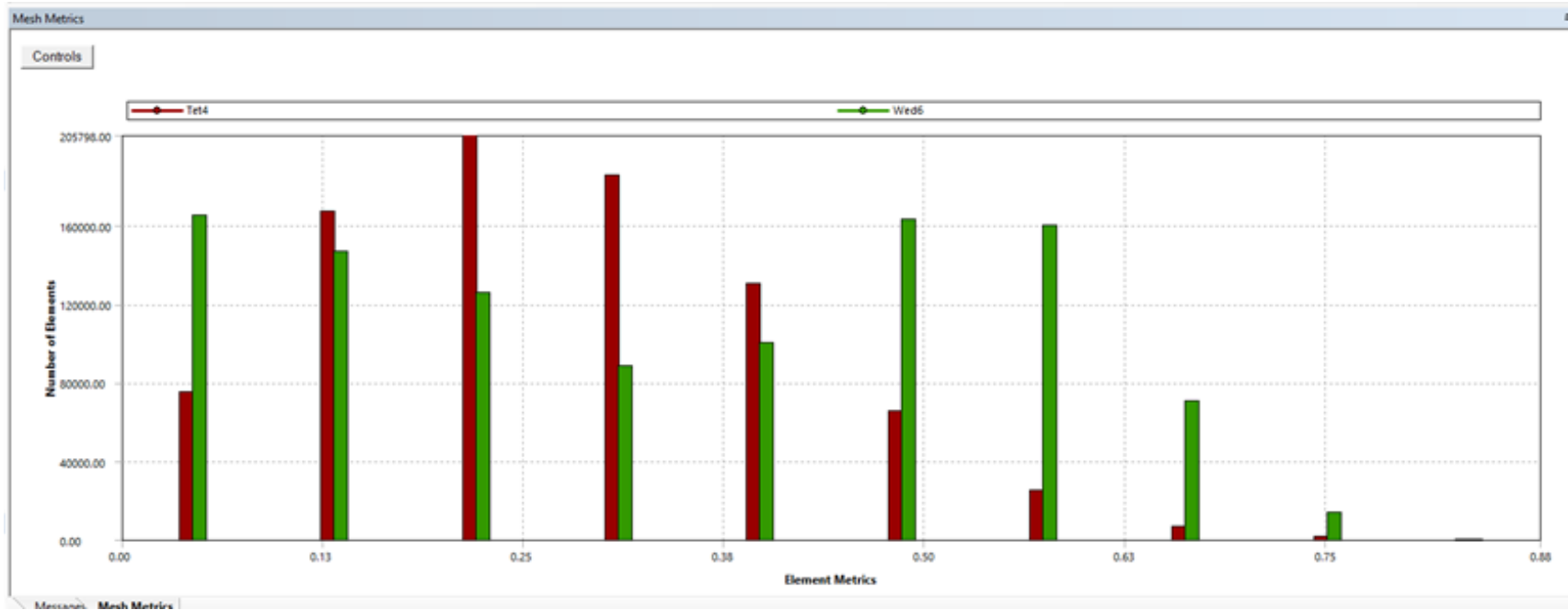


Figure 14: Mesh Skewness Bar Graph

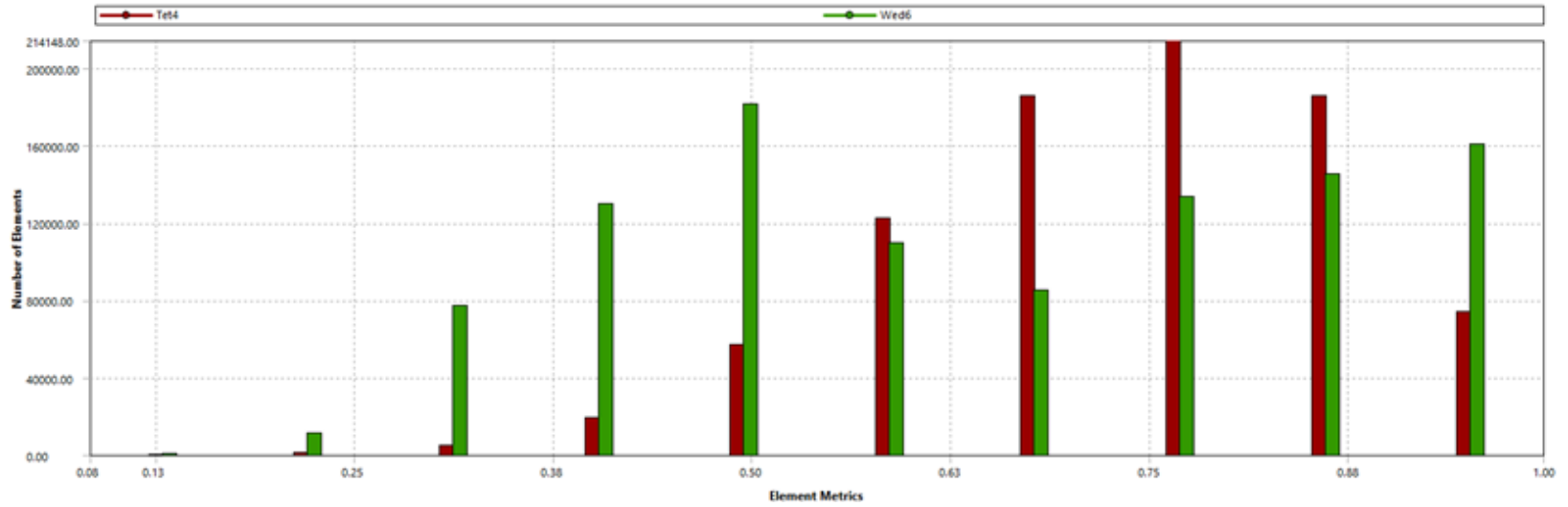


Figure 15: Mesh Orthogonality Bar Graph

As the mesh is created for the twin gear set, there are thin areas surrounding the gears that require a finer mesh. This is due to the small gaps between the teeth and the speed at which the gears rotate. An image of these areas can be seen in Figure 16.

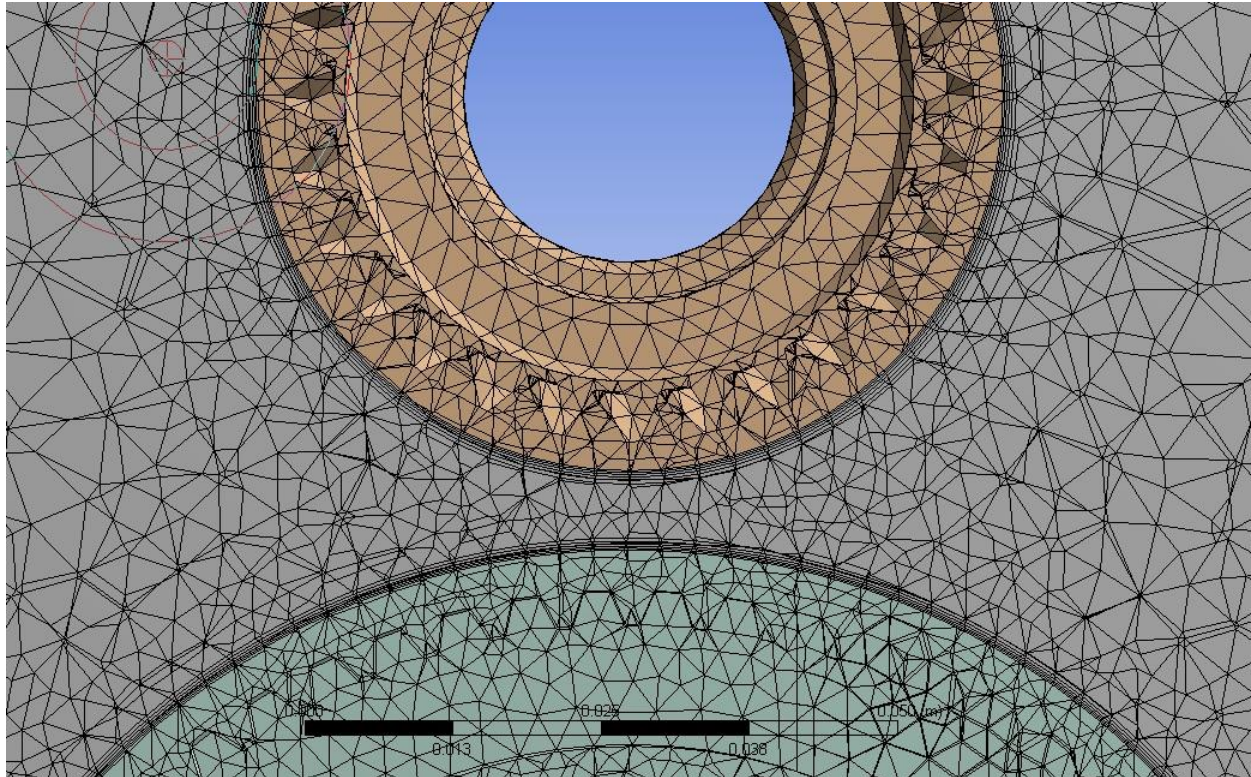


Figure 16: Fine Detail Area of Mesh

This area of the mesh must be finer for suitable skewness and orthogonal quality. The geometry was created with this need in mind and the section near the gears, colored green and orange in Figure 16, is a separate part from the rest of the inside of the gearbox. This allows the finer mesh to be created more easily.

Regions where large speed differentials occur also require special attention. In the present system, large speed differentials occur around the edge of the fine mesh area, at the

gears and at the walls of the enclosure of the gearbox. These regions are labeled 1,2, and 3 respectively in Figure 17.

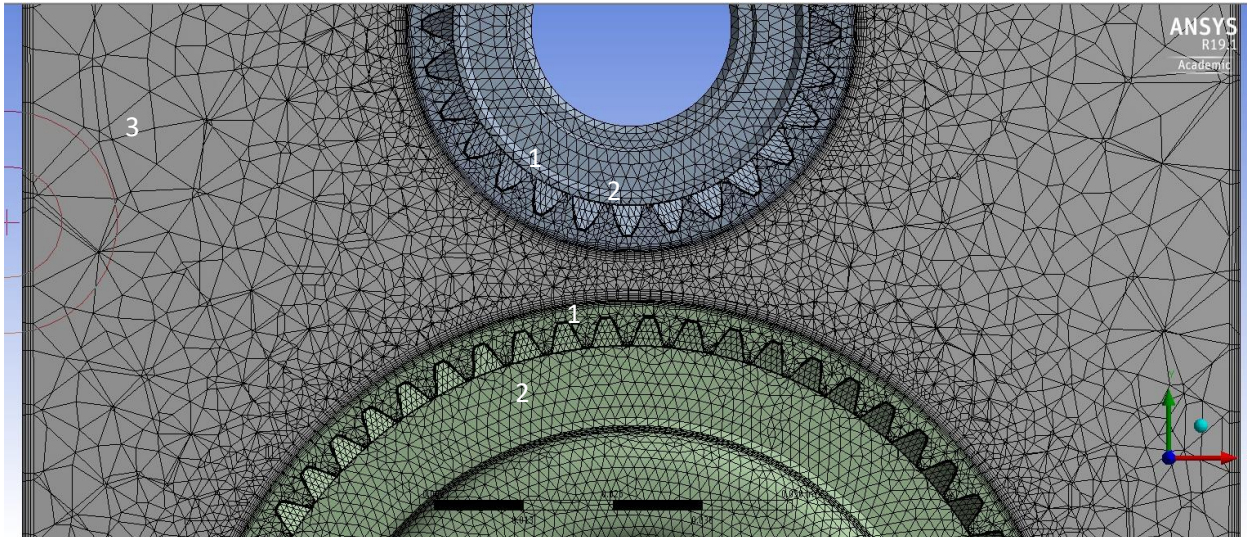


Figure 17: Fine Mesh Areas of the TGB Gearbox

Prism layers were added to the model in areas with large speed differentials. Prism layers are elements of mesh that take the volume mesh near the boundary and make layers of orthogonal prism cells from their faces. An example of a prism layer can be seen in Figure 18. Prism layers can be generated in several different ways: first layer thickness, total thickness, smooth transition, first aspect ratio and last aspect ratio. The *first layer thickness* method allows the number of layers, the thickness of the first layer and the percent growth to be defined. The *total thickness* method is similar to the *first layer* method, except instead of the first layer thickness being defined, the total thickness of the prism layers is defined. The smooth transition type creates prism layers that smoothly change volume between layers. *First aspect ratio* uses a ratio between the inflation layer height and base size. *Last aspect ratio* creates prism layers based on the last aspect ratio and the first layer height [43]. Prism layers

allow the speed of the fluid to be more easily transitioned because of the larger number of small cells near the boundary without increasing the number of cells on the surface of the boundary surface.

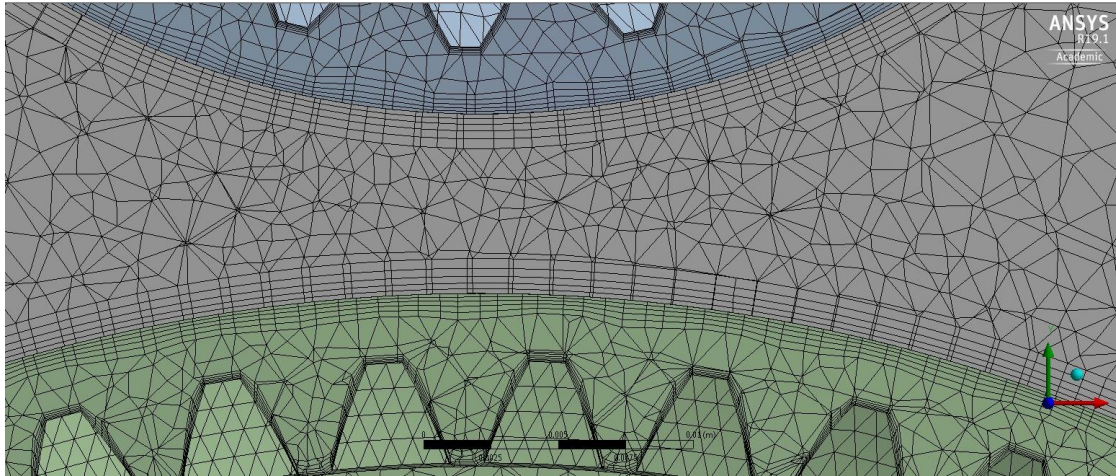


Figure 18: Prism Layers

For the TGB gear set the settings for the mesh are: 0.002 m size and curvature turned on (global settings). For local settings, the rotating driving fluid and pinion fluid have a size of 0.0015 m and curvature and proximity settings. Curvature settings refines the mesh around curves for a better fit, while proximity settings refine mesh in areas that are in close proximity to other objects, for example the area near the interface between the rotating fluid and the main gearbox. The faces of the fluid body that are along the interface also have a size of 0.0015 m, and curvature and proximity turned on. There are inflation layers set at the enclosure walls, the walls of the gears and on both sides of the interface. The inflation layers use a total thickness value of 1.3 mm. This value was chosen to match the inflation layers of the Star CCM+ model. Overall, this causes the mesh to have about 2 million elements. Inflation layers had to be added to the enclosure walls due to the large speed differential encountered and the

fact that the speed of the fluid must decrease to zero at the walls. Inflation layers were also added to the walls of the gears. This was due to the spatial resolution needed in the simulation in this region. Layers were also added to the interface zone. The rotating fluid bodies and the face of the fluid body along the interface required smaller mesh elements due to the spatial resolution needed in these areas during the simulation.

4.2 Single Gear Box (SGB)

4.2.1 Geometry

For the optimization study the twin gear (TGB) gearbox was simplified to a single gear box (SGB), as described in Chapter 3.

4.2.2 Mesh

The SGB simplification was made due to prohibitively large number of mesh elements, at least four million, that would have been needed for the twin gear configuration. In the SGB the driving gear is removed from the gearbox, which removes one area that needs a refined mesh for the simulation and therefore reduces the required number of mesh elements.

The information used to create the mesh for the TGB was adapted for the SGB. The global settings were that the mesh size was 0.003 m with curvature turned on. For local settings the rotating fluid had a size of 0.0015 m and curvature and proximity settings. The faces of the fluid body that were along the interface also had a size of 0.0015 m, and curvature and proximity turned on. There were inflation layers set at the enclosure walls, the walls of the gears and on both sides of the interface. The inflation layers used total thickness with a thickness of 1.6 mm. This was chosen to match the inflation layers of the Star CCM+ model.

The face along the gear was set to have a mesh size of 0.0006 m, this was to allow for better detail around the gear teeth. An inflation layer with a total thickness of 0.0006 m was also added at the surface of the gear. Overall, this results in a mesh of about 1.8 million elements. Inflation layers had to be added to the enclosure walls due to the large speed differential and the fact that the speed of the fluid must decrease to zero at the walls. Another area that had inflation layers added was the interface zone, as seen in Figure 19. This area had a large speed differential, due to the method that the simulation used to model the rotation of the gear.

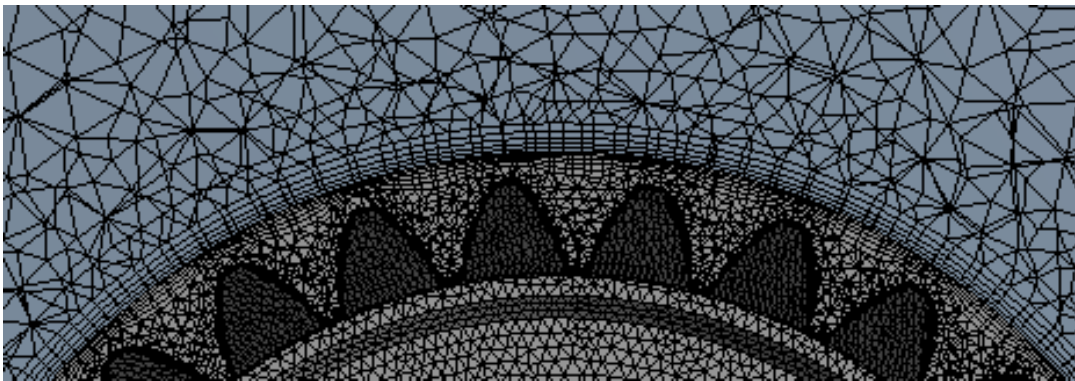


Figure 19: Inflation Layers Added to Single Gear

4.3 CFD Solver

4.3.1 Solver Type

There are two solver types used in Ansys Fluent, one is a pressure solver, while the other is a density solver. According to Ansys [44] the density-based solver uses the momentum equations to determine the velocity field and uses the continuity equation to determine the density field. The density-based solver then uses the equation of state to determine the pressure field. The pressure-based solver uses a pressure correction equation to solve for

pressure. For this simulation a pressure-based solver is used. This is because a density-based solver cannot be used for multiple fluid simulations.

4.3.2 Models

When a simulation is set-up different models must be defined. For the TGB model and the SGB model, the multiphase model and the viscous model are changed. The multiphase model is set to *volume of fluid* with an explicit formulation and an implicit body force. The number of phases is set to *two* for oil and air. The implicit body force was turned on due to account for gravity. The viscous model was changed from the default of laminar to a k-epsilon realizable method. These settings were chosen to match the high-fidelity Star CCM+ model. Within the viscous model the near-wall treatment was also chosen. There are multiple near wall treatments including Standard, Scalable and Enhanced Wall Treatment. The main way to determine which of these three methods to choose is to look at the y^+ value, which defines a dimensionless wall distance for wall-bounded flow [45].

$$y^+ = \frac{u_* \times y}{\nu} \quad (22)$$

In Eq. (22) u_* is the friction velocity, y is the distance to the nearest wall and ν is the kinematic viscosity. The smaller y^+ values should use enhanced wall treatment, while the larger y^+ values should use standard wall treatment.

In Ansys if the y^+ value is less than 1 the enhanced wall treatment should be used, if the y^+ value is greater than 30 the standard function should be used, and if the y^+ value is between 0 and 30 the scalable wall function should be used [46]. For this model the y^+ values are around 10 and therefore the scalable wall function was used in the *SGB model*.

4.3.3 Boundary and Cell Zone Conditions and Movement

The boundary conditions must be defined for the simulation. There are multiple types of boundary conditions. For the TGB and the SGB model simulations the two types of boundaries for faces are wall and interface. The interface boundary is used between the rotating mesh section and the rest of the gearbox, as seen in Figure 20 for the SGB and Figure 21 for the TGB. The rest of the faces are treated as walls.

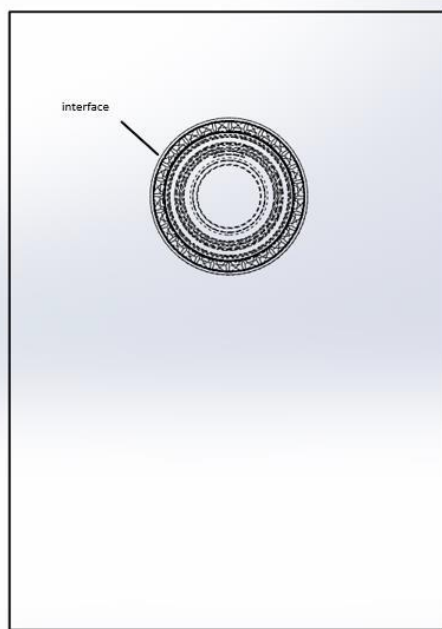


Figure 20: Single Gear Interface

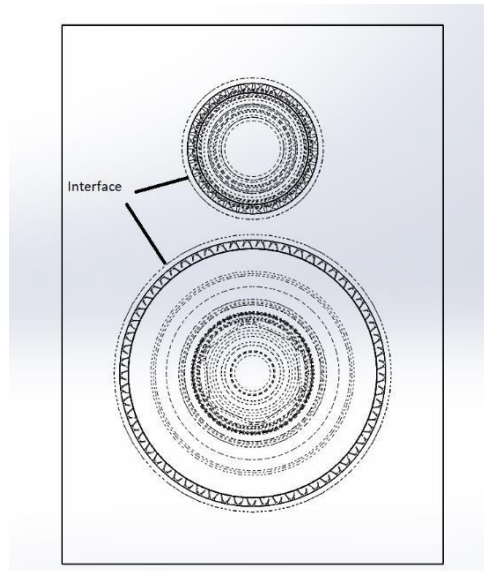


Figure 21:TGB Interface Boundaries

Next, the movement of the gears is defined. There are two methods used to simulate a gear's rotation: sliding mesh and dynamic mesh. Dynamic mesh is where the mesh is changed as the gears move, whereas sliding mesh is where a section of mesh is moved at the speed of the gear to simulate the gear movement, but the mesh is not actually changed.

There are advantages and disadvantages to both types of movements. For the twin gear set the largest advantage of dynamic mesh is that the gear teeth can be intermeshed, whereas its biggest disadvantage is the time-consuming nature of the associated simulation and small time-steps needed. This requires more time-steps to rotate the gear, which increases the computation time.

The main advantage of the sliding mesh is that simulations are less time-consuming and can handle larger time-steps. The mesh is not changed, just rotated, which takes less time than regenerating a mesh after every time-step. The disadvantage of the sliding mesh is that it is not as easy to have the gear teeth intertwine to match the physical TGB gearbox.

4.3.4 Solution Methods

Several different algorithms can be used in Ansys Fluent for a pressure-based simulation. Each algorithm is best suited for a specific scenario. The four different types are SIMPLE, SIMPLEC, PISO, and FSM. FSM is the Fractional Step Method and is only available for time-dependent flows [47]. SIMPLE is the default algorithm and is most generally used for steady-state calculations. SIMPLEC also is used mostly for steady-state calculations but differs from SIMPLE by the larger under-relaxation values that can be applied. *Under-relaxation* values are used by the solver to help the solution converge by making the solution more stable. PISO is most generally used for transient calculations. PISO resembles SIMPLE and SIMPLEC, but it has skewness correction and neighbor correction. For the present simulations the SIMPLE algorithm was selected, this was chosen from trial and error method. When PISO was used more divergence issues occurred than when the SIMPLE method was used.

When a solutions' residuals are irregular and rough, changing the under-relaxation values can cause the residuals to smooth. There are *under-relaxation* factors for pressure, density, body forces, momentum, turbulent kinetic energy, turbulent dissipation rate, and turbulent viscosity. When creating a simulation, the first tries should always leave the under-relaxation factors at the defaults. The under-relaxation factors should only be changed when the solution has trouble converging. As under-relaxation factors decrease in value, the solution time can increase due to the more complicated calculations. For the twin-gear simulations, the under-relaxation values used can be found in Table 3. The one gear simulation under-relaxation factors can be found in Table 4

Table 3: Under-Relaxation Factor Values

Under-Relaxation Values	
Pressure	0.009
Density	0.8
Body Forces	0.8
Momentum	0.01
Turbulent Kinetic Energy	0.1
Turbulent Dissipation Rate	0.1
Turbulent Viscosity	0.8

Table 4: Under-Relaxation Values for the One Gear Simulation

Under-Relaxation Values full driven gear with axle	
Pressure	0.01
Density	0.8
Body Forces	0.8
Momentum	0.01
Turbulent Kinetic Energy	0.35
Turbulent Dissipation Rate	0.3
Turbulent Viscosity	0.8

The *cycle type* setting can also be changed to help the solution converge. Cycle type is how the simulation reads data for the multigrid solver. There are flexible, V, W and F cycle types. The cycle type can be defined for pressure, x-momentum, y-momentum, z-momentum, turbulent kinetic energy and turbulent dissipation rate. The default for each in Fluent is v-cycle for pressure and flexible cycle for the others. For each variable that is not set to flexible cycle there is a stabilization method that can be used bi-conjugate gradient stabilized method (BCGSTAB), recursive projection method (RPM) and for pressure CG. Changing the cycle type and the stabilization method can affect the convergence of the simulation.

4.4 Fidelity versus Computing Time

When creating a computer model two factors must be considered: model fidelity and the time required to perform the simulation. Higher fidelity simulations usually have larger computing times. The balance between model fidelity and computing time is unique to each simulation and must be found by considering the importance of how accurate the simulation should be and the importance of completing the simulation in a certain amount of time.

When finding this balance, the acceptable accuracy of the simulation must be considered, otherwise the simulation is no longer a useful tool for the research. One way to ensure accuracy is to perform a grid independence study. A grid independence study is a way to make sure the results of the simulation are not based on the size of the mesh. This can be accomplished by running the simulation with the desired mesh size, and then rerunning the simulation with a mesh of smaller elements to make sure that the results are within a reasonable amount of each other [48]. Also, the computing time must not be allowed to become unreasonable. This too would cause the simulation to become a less useful research tool.

Because optimization is a critical component of this research, computing time was weighted heavily when determining this balance. While the simulations must still be accurate to obtain useful results, computing time must be as small as possible to enable an iterative optimization study. The TGB model took around seven days to compute one revolution of the pinion gear, this lengthy simulation time was a prime factor in using the SGB model for the

optimization. In comparison the SGB model took three and a half to four days to complete one rotation of the pinion gear. This was about half of the computation time of the TGB model.

5. Simulation Results

5.1 Simulation Progression

To reach the simulation of the TGB gearbox, a series of models of increasing complexity were investigated. The first models created were for rotating cylinders in the enclosure without an axle, followed by a rotating cylinder with an axle. Once these simple simulations were created, the cylinders were made more complex by adding four teeth. At this point of the process of creating the TGB gearbox simulation, the simulations diverged onto parallel paths. One path was with two rotating cylinders with axles while the other was one full helical gear, the pinion gear from the TGB gearbox without and then with an axle. The progression of the simulation can be seen in Figure 22.

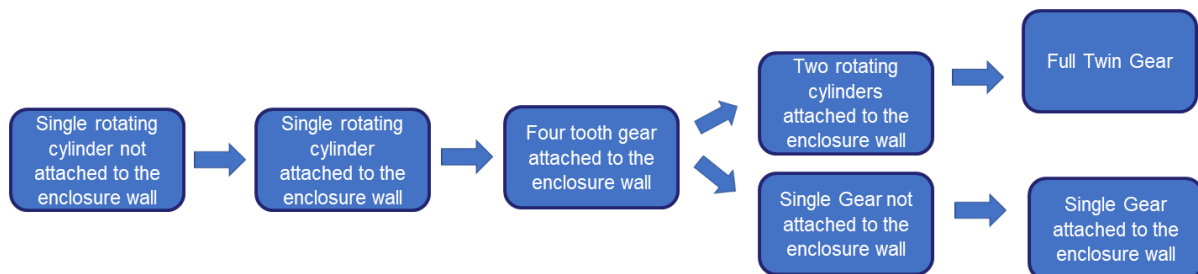


Figure 22: Simulation Progression

The single rotating cylinder not attached to the enclosure wall (no axle) seen in Figure 23, was the simplest version that was simulated. The simulation was considered a success if the “gear” was able to rotate a full 360 degrees.

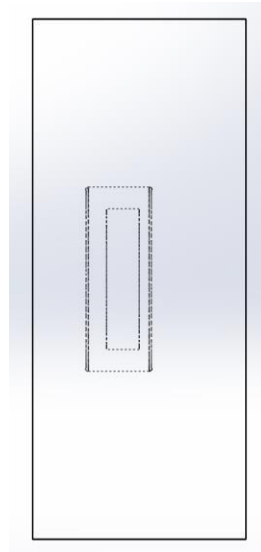


Figure 23: Single Rotating Gear not Touching the Enclosure (No Axle)

This simulation was created by leaving most Fluent settings at default and only changing the under-relaxation values with the pressure as a flexible cycle. Under-relaxation values are used by the solver to help the solution converge by making it more stable. There were several iterations of running the simulation and changing the under-relaxation factors as various obstacles occurred. These under-relaxation factors used can be seen in Table 5. For the rotating cylinder attached to the enclosure wall (with axle) seen in Figure 24, the same settings for the pressure cycle type and under-relaxation values were used.

Table 5: Under-Relaxation Values for Rotating Cylinder

Under-Relaxation Values rotating cylinder no axle	
Pressure	0.3
Density	0.8
Body Forces	0.8
Momentum	0.5
Turbulent Kinetic Energy	0.5
Turbulent Dissipation Rate	0.5
Turbulent Viscosity	0.8

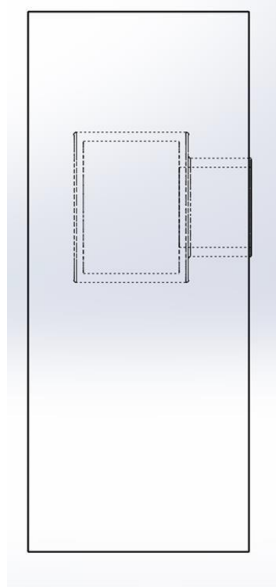


Figure 24: Single Rotating Gear with Axle

Once the single rotating cylinder (both with and without axle) was simulated correctly a four- tooth gear without an axle was simulated.

Using the same dimensions for the four-tooth gear as the pinion gear, only with fewer teeth, a model was created using SolidWorks seen in Figure 25. This model was then simulated with Ansys Fluent. The original settings for the four-tooth gear model were the same under-relaxation factors as the single rotating cylinder with axle. As problems arose the under-relaxation factors and cycle settings were changed. The under-relaxation factors for this model are in Table 6.

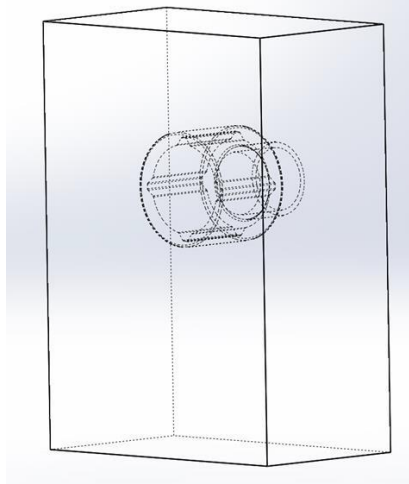


Figure 25: Four Tooth Gear

Table 6: Under-Relaxation Factors for Four Tooth Gear

Under-Relaxation Values four teeth without axle	
Pressure	0.3
Density	0.8
Body Forces	0.8
Momentum	0.1
Turbulent Kinetic Energy	0.4
Turbulent Dissipation Rate	0.4
Turbulent Viscosity	0.8

Once the four-tooth model complications were resolved, the simulation path was split into two parallel paths. The first path was to simulate the single full pinion gear from the TGB gearbox without an axle. The second was to simulate two rotating cylinders. This split in the path was used to determine which complications arose due to the teeth of the gear and which complications arose from the gap between the two gears and the more complicated fluid flow. These two paths were investigated simultaneously using multiple computers. The single pinion gear model can be seen in Figure 26.

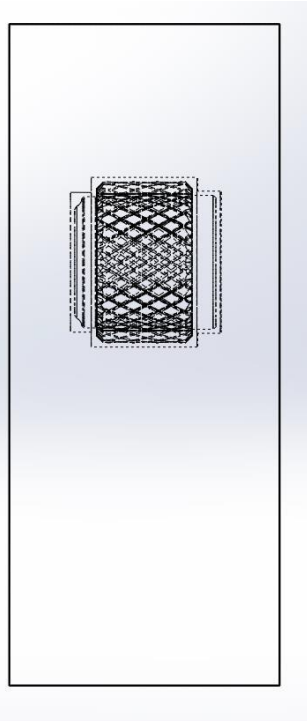


Figure 26: Pinion Gear without Axle

The single pinion gear model was more complicated than the four-tooth gear model, due to the increased number of teeth and the change from spur to helical gear. The first run of the simulation of the pinion gear model used the settings from the four-tooth gear model, but due to the more complicated nature of the model, adjustments were made to resolve multiple problems. The under-relaxation factors were adjusted, the final under-relaxation values are given in Table 7.

Table 7: Under-Relaxation Factors of Pinion Gear without Axle

Under-Relaxation Values full driven gear without axle	
Pressure	0.05
Density	0.8
Body Forces	0.8
Momentum	0.07
Turbulent Kinetic Energy	0.35
Turbulent Dissipation Rate	0.35
Turbulent Viscosity	0.8

After completion of the pinion gear model simulation, an axle was added to the system, shown in Figure 27. The first simulation of the pinion gear with an axle used the settings that were found for the pinion gear without an axle, the under-relaxation factors were then changed as needed, the final values of which are in Table 8. Various simulations of the pinion gear axle system were run, including full immersion and also two fluids, that is, under dip lubrication.

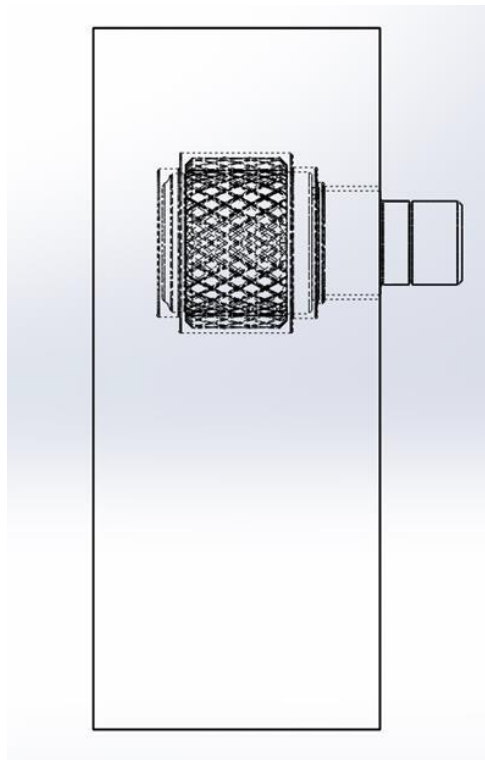


Figure 27: Driven Gear with Axle

Table 8: Under-Relaxation Factors of Driven Gear with Axle

Under-Relaxation Values full driven gear with axle	
Pressure	0.01
Density	0.8
Body Forces	0.8
Momentum	0.01
Turbulent Kinetic Energy	0.35
Turbulent Dissipation Rate	0.3
Turbulent Viscosity	0.8

The simulation development path parallel to the one just described is the simulation of two cylinders and then the full TGB gearbox seen in Figure 28. The under-relaxation values found while performing the two cylinder simulation are found in Table 9 , while the under-relaxation values found while performing the full TGB gearbox are found in Table 10.

Table 9: Under-Relaxation Values for the Two Cylinder Model

Under-Relaxation Values Two Cylinders	
Pressure	0.1
Density	0.8
Body Forces	0.8
Momentum	0.01
Turbulent Kinetic Energy	0.4
Turbulent Dissipation Rate	0.4
Turbulent Viscosity	0.8

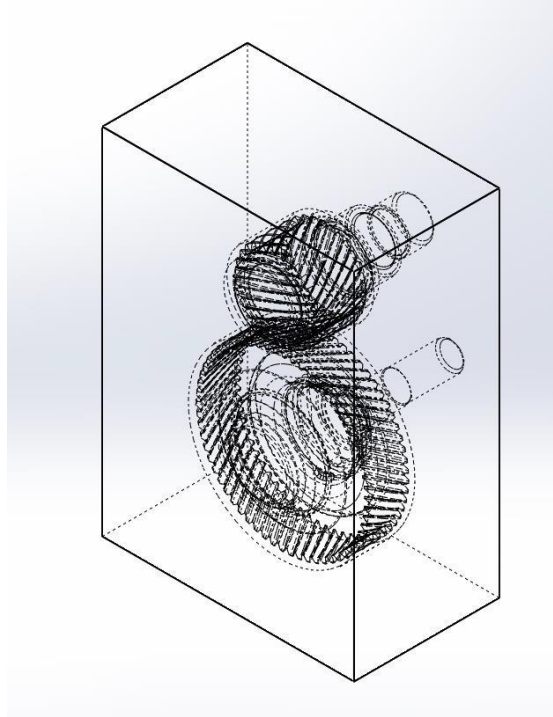


Figure 28: Full TGB Gearbox

Table 10: Under-Relaxation Factors of Full TGB Gearbox

Under-Relaxation Values full FZG gearbox	
Pressure	0.01
Density	0.8
Body Forces	0.8
Momentum	0.01
Turbulent Kinetic Energy	0.1
Turbulent Dissipation Rate	0.1
Turbulent Viscosity	0.8

While performing the simulation of the full TGB gearbox, it was found that the timestep size and mesh element size needed for the simulation to run caused the calculation time to be large: seven days for a single rotation of the pinion gear. This large calculation time was not feasible for an optimization study. Therefore, the single gear with an axle (the SGB model) simulation that was the final step in the first branch of the simulation progression was used for

the optimization. The calculation time of the SGB model was about half that of the TGB model, this allowed for the calculations to be completed in a more reasonable time limit.

5.2 Obstacles and Solutions

Several common obstacles were found throughout the simulation progression. The main obstacle was divergence in the residuals instead of convergence. The two most common residuals that diverged were pressure and momentum. Another obstacle was the return of NaN (not a number) for results. The most common obstacle was the Global Courant number becoming too large.

Both the pressure and momentum divergences occurred throughout the simulation progression, starting at the four-tooth simulation. There were several methods to overcome this obstacle. The first is to ensure that there are inflation layers at the walls, interface, and gear. These areas, especially the outer gearbox walls, can have large velocity differentials. By including inflation layers at the walls, interface, and gear the likelihood of divergence decreases. It is still possible to have the simulation diverge after inflation layers are added. When this occurred, the under-relaxation values were reduced for the diverging residuals. The divergence can also be overcome by changing the cycle type and the correction type for the cycle type. The majority of the divergence was associated with pressure and momentum, but turbulent kinetic energy and turbulent dissipation rate were other sources for it.

One of the major issues found when creating the simulation was that the Global Courant number exceeded the Ansys Limit of 250. A Global Courant number is a dimensionless number that compares the characteristic time of a fluid over a control volume with the time step [49].

The characteristic time is found with Equation 23, where V_{cell} is the cell volume and w_{face} is the volume flow rate on each face.

$$t_{char} = \text{Min} \left[\frac{V_{cell}}{w_{face}} \right] \quad (23)$$

The Global Courant number is calculated by dividing the time step by the characteristic time. The Global Courant number can become too large if the time step is too large or if the characteristic time is too small. To overcome this problem, the simulation uses a variable time step. Although reducing the timestep can help keep the Global Courant number in check the reduction in time step size increases the computing time. This is because a smaller time step means that more timesteps are needed to reach the completed time.

5.4 Results

The results presented are not comparable to the results obtained with the high-fidelity Star CCM+ model or those from the experimental TGB gearbox because the simulations did not reach steady-state in the available solution time. With Star CCM+ the steady state of the TGB gear pair was reached after the simulation completed 15-20 rotations. In contrast, the results herein are taken at 0.113 seconds or about 2.46 rotations, which took about 4 weeks to reach. The baffle clearances used in the single gear simulation were 114.29 mm, 89.29 mm, 64.29 mm, and 39.29 mm. These locations were chosen due to their even spacing throughout the gearbox.

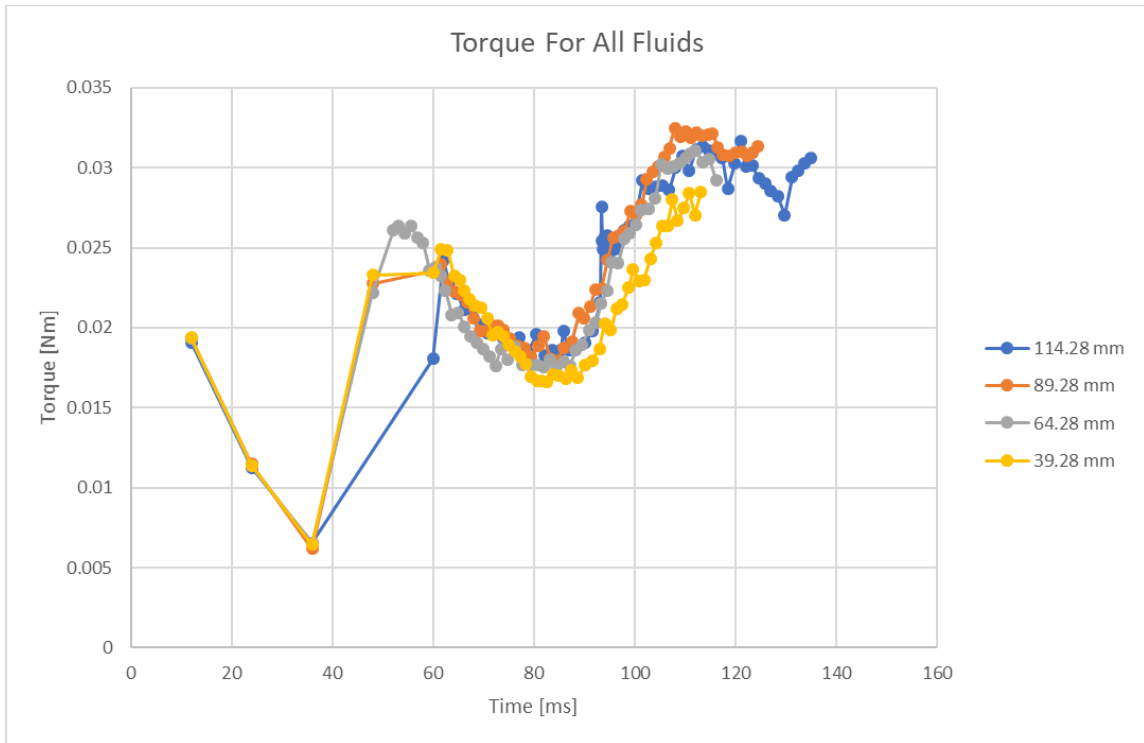


Figure 29: All Fluids Torque for Each Baffle Location

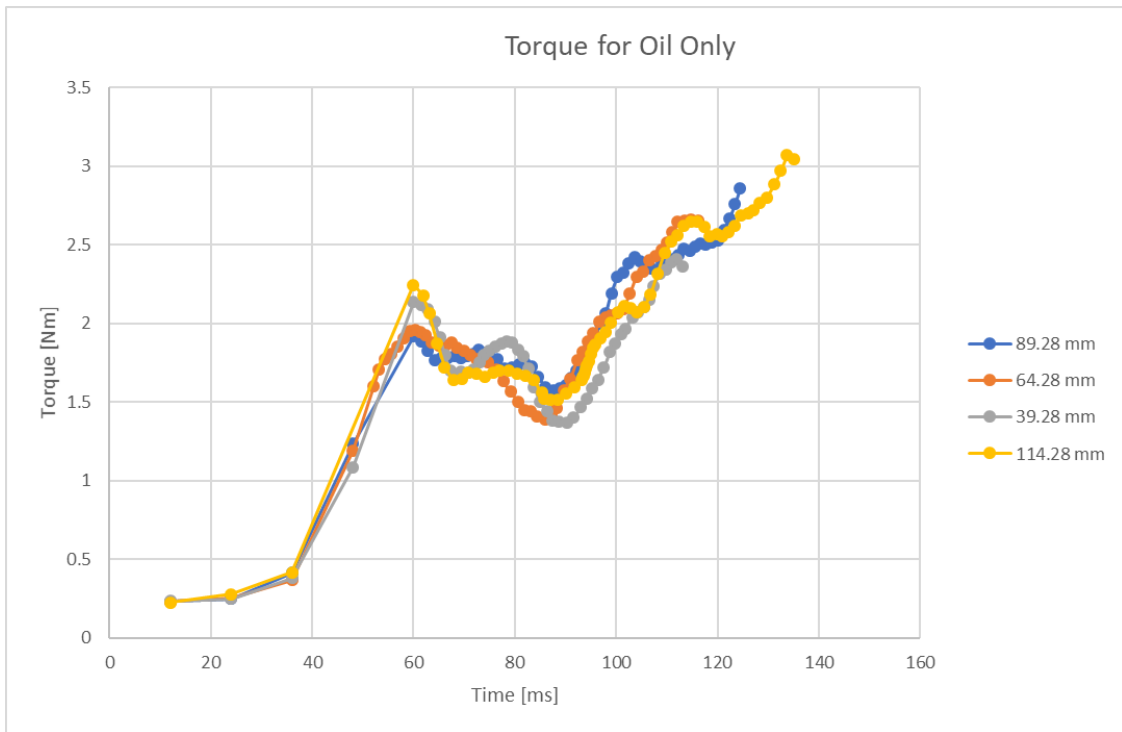


Figure 30: Oil Only Torque for all Baffle Locations

The magnitudes of the torque consumed with each baffle clearance over time are shown in Figure 29 and Figure 30; the magnitudes were calculated using Ansys CFD Post Processing. The difference between the two torques are that in Figure 29 both air and the oil are considered while in Figure 30 only the oil is considered. In CFD Post Processing the torque is calculated by the cross product of the force at each element and the moment arm from the center of rotation to the element. The force in CFD Post processing is calculated using the pressure and the shear force. The torque shown is about the z-axis because it is the rotation axis. Ansys CFD Post processing calculates the torque for all fluids, both oil and air, by calculating and then summing the torque for both oil and air. It can be observed in Figure 29 and Figure 30 the magnitude of the oil only torque is much larger than the oil and air combination. This is caused by the torque consumed by air and the torque consumed by oil being of similar magnitudes but opposite signs. This does not make physical sense. This problem might be caused by limitations in our current understanding of the post-processing routine and is currently being investigated directly with Ansys. As seen in the figures, the gear is not in steady state for either the oil only torque or the oil and air torque. The figures above also show that the torque is different at each baffle location, although the overall pattern is similar.

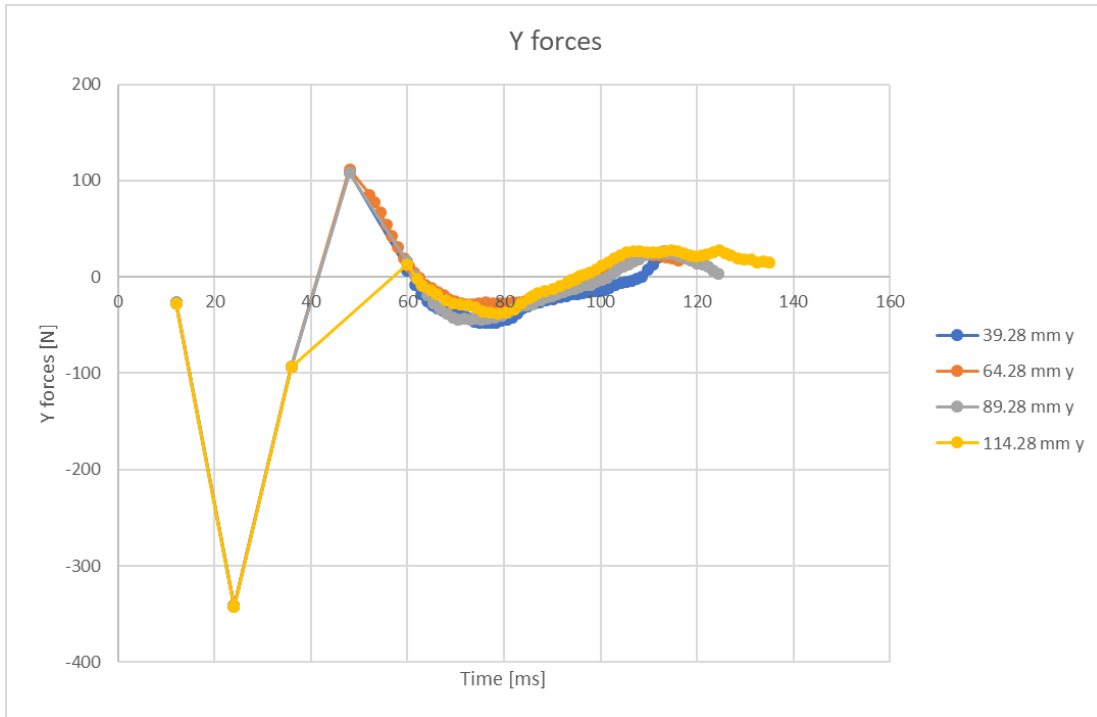


Figure 31: Y Forces on Gear for Each Baffle Clearance

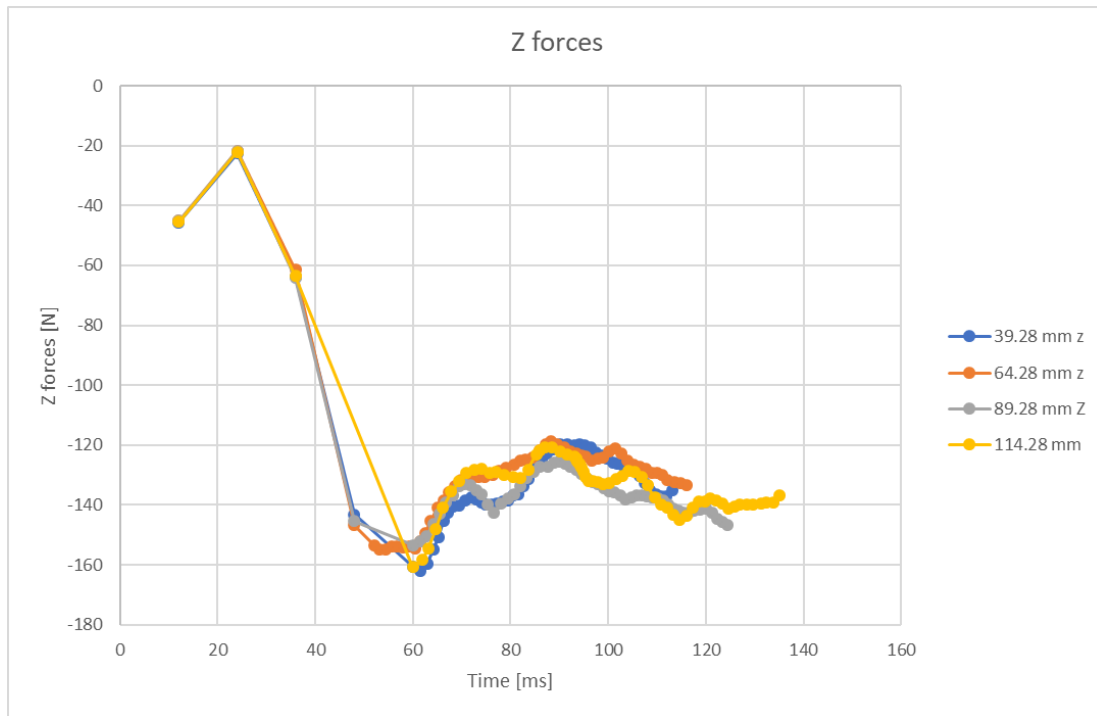


Figure 32: Z Forces on Gear for Each Baffle Clearance

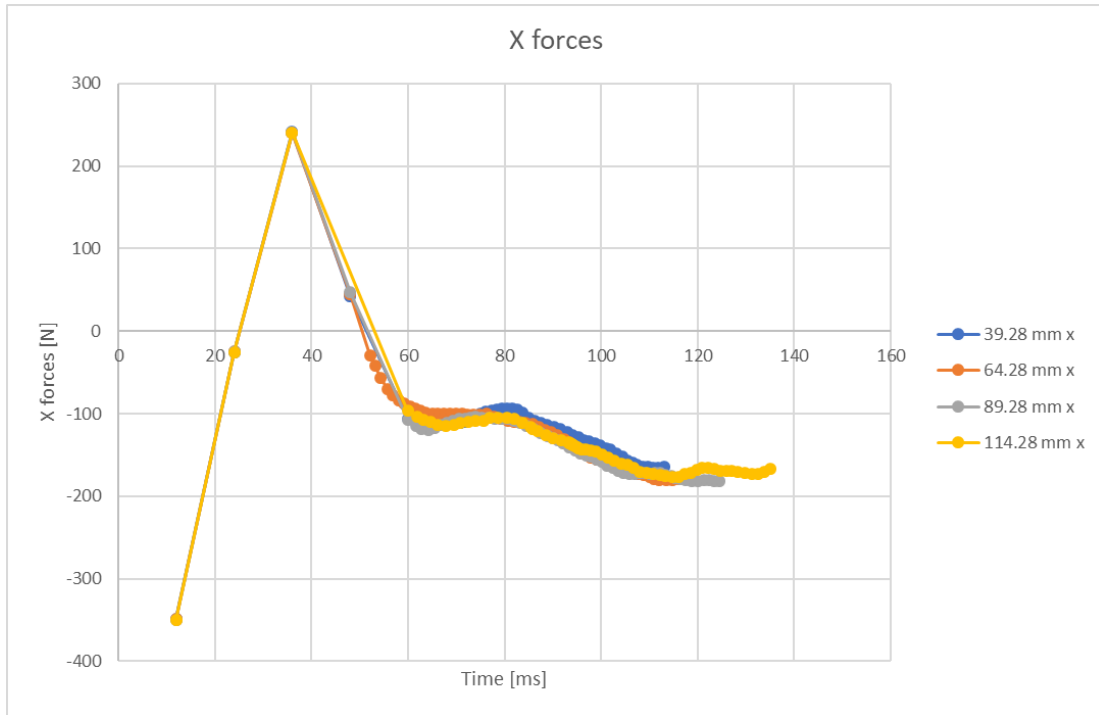


Figure 33: X Forces on Gear for Each Baffle Clearance

Figure 31, Figure 32, and Figure 33 display the sum of the forces on the gear in each direction. These forces were calculated using Ansys CFD Postprocessing and only include the forces of the oil. The force figures show that the forces for a baffle location exhibit similar patterns but are different between each baffle location.

6. Optimization

Due to the transient nature of the data, the integration of the torque data over time, which is proportional to the energy consumed data, will be used for the optimization instead of the torque at a single point in time. The energy consumed data, used for optimization, is calculated from the results in Chapter 5. Baffle clearances that cause possible minimum and maximum energy losses are identified through the optimization process.

6.1 Churning Loss Optimization

Due to the transient nature of the simulation results available, the optimization to be presented considers the data over time. The torque data were numerically integrated over time using Eq. (24), where Δt refers to the change in time and T refers to the torque, to find the energy, normalized to angular velocity, approximation.

$$E_v = \sum_{k=1}^N \left(\frac{T_{k-1} + T_k}{2} \Delta t_k \right) \quad (24)$$

By using the area under the curve of torque data an approximate of the energy used as the gear is turned can be found. The power itself isn't necessary to compute energy because the speed is constant over time, this means that the torque data and power data have the same pattern and are related by a scaling factor, the angular velocity, that is consistent over all time and for all baffle locations.

The torque data in Figure 29 is numerically integrated over a common time span from zero to 0.113 seconds (the amount of time that the simulation data is available for all baffle

locations) and the results are shown in Table 11 and Figure 34. The energy data is the angular velocity normalized energy.

Table 11: Air and Oil Energy Consumed

Baffle Location (mm)	Baffle Clearance (mm)	Energy (J/(rad/s))
25	114.29	0.00185
50	89.29	0.00203
75	64.29	0.00200
100	39.29	0.00188

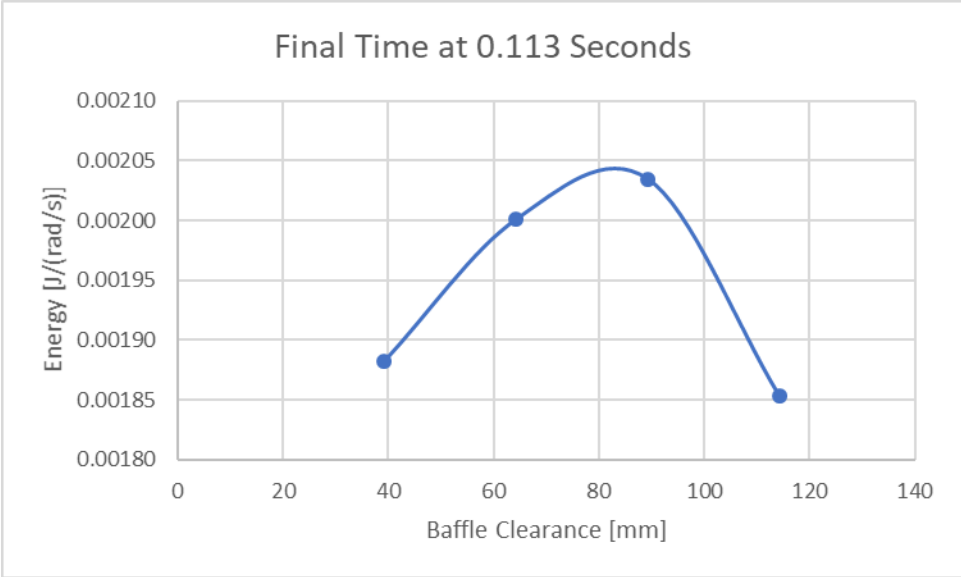


Figure 34: Single Gear Energy Consumption for both Air and Oil at 0.113 Seconds

The energy data is used to investigate the locations of possible minima and maxima. Using the optimization process described in Figure 35. To perform the optimization a polynomial E_v is fit to the energy consumed data.

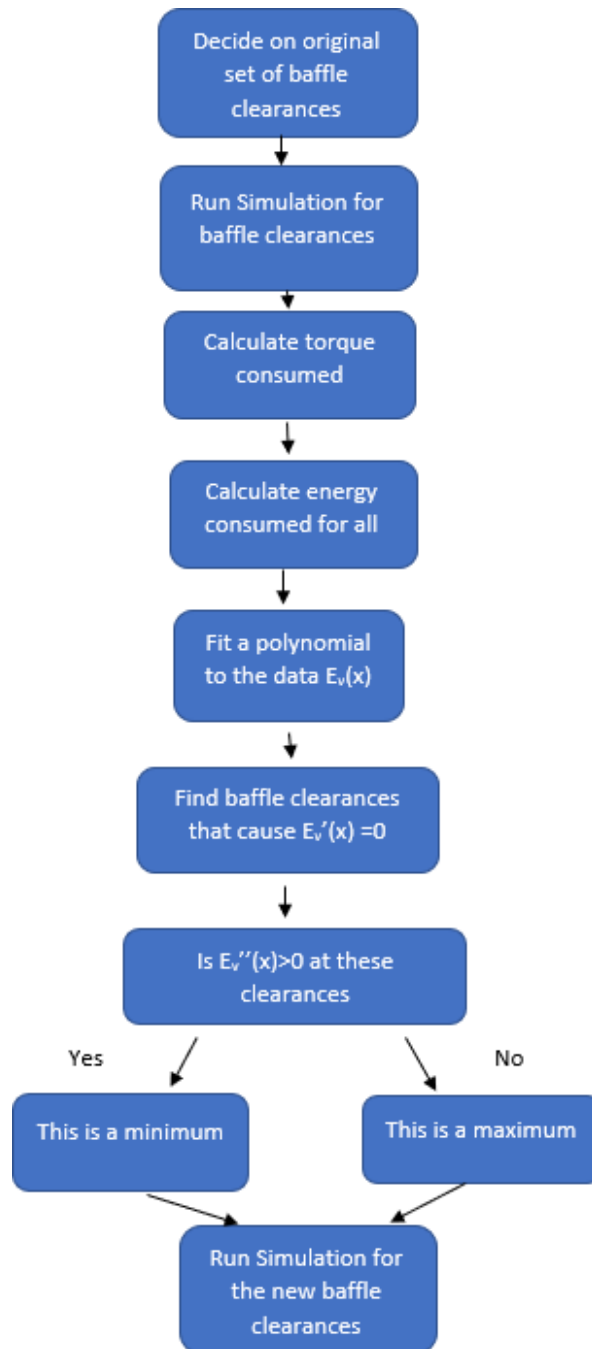


Figure 35: Optimization Algorithm Flowchart

A polynomial is fit to the energy data resulting in

$$E_v = -\frac{6.717e15x^3}{4.836e24} + \frac{3.786e15x^2}{1.8889e22} - \frac{5.473e15x}{1.181e21} + \frac{8.483e15}{4.612e18} \quad (25)$$

In Eq. (25) x is the baffle clearance. By observation of Figure 34 there are possible minima points with a baffle clearance either larger than 114.29 mm or less than 39.29 mm. There is also a possible maximum energy consumed point at a clearance of about 85 mm. A MATLAB code, provided in Appendix A, is used to find the maximum.

The maximum value is obtained by taking the derivative of the curve and solving for the position at zero slope or maxima point. This is equivalent to solving the optimization problem of maximizing the energy subject to Eq. (25). The results of the analysis show that there is a possible maximum with a clearance of approximately 83.29 mm (which is a baffle location of 56 mm).

If the simulation had reached steady-state, the torque at a final time during steady-state would be sufficient for finding the minima and maxima points of power loss. Since all baffle location simulations have the gear rotating at the same speed, torque follows the same pattern as power. To illustrate using the torque at the final time here, the torque data that would be used is shown in Table 12 and Figure 36.

Table 12: Single Gear Torque at 0.113 Seconds for Oil and Air

Baffle Location (mm)	Baffle Clearance (mm)	Torque (Nm)
25	114.29	0.03136
50	89.29	0.03201
75	64.29	0.03032
100	39.29	0.02850

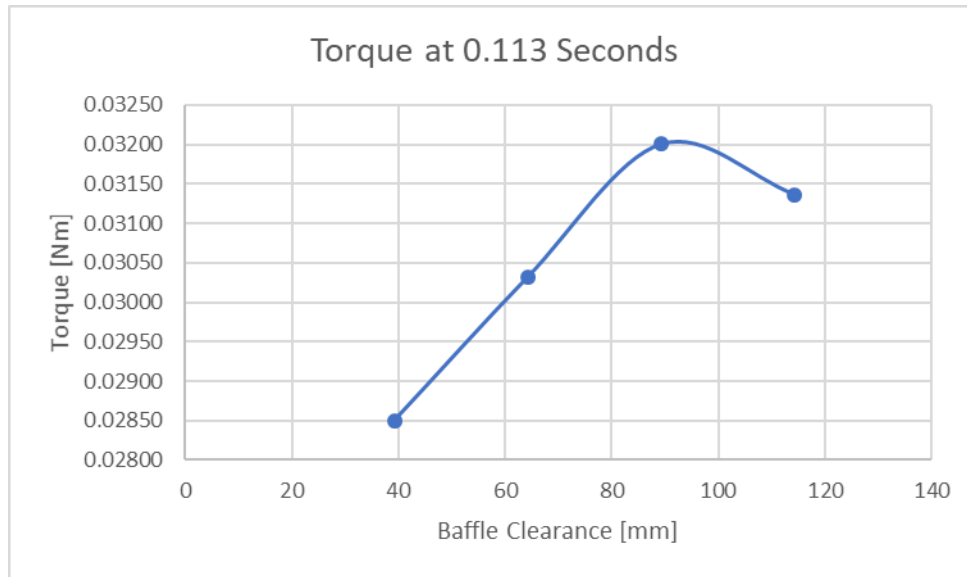


Figure 36: Single Gear Torque for Oil and Air at 0.113 Seconds

The problem is finding the maxima and minima torque (power surrogate) with respect to the baffle clearance. A polynomial fit to the data results in

$$T = -\frac{7.066e15x^3}{3.022e23} + \frac{5.194e15x^2}{1.181e21} - \frac{3.522e15x}{1.845e19} + \frac{8.827e15}{2.882e17} \quad (26)$$

As seen in Figure 36 a clearance less than 39.29 mm could be a minimum torque consumed.

The maximum value is obtained by taking the derivative of the curve and solving for the position at zero slope or maxima point. A MATLAB code, provided in Appendix C, is used to find the maximum of the curve. The results of the analysis show that there is a possible maximum with a clearance of 97.53 mm. This clearance is about 14 mm different than the maximum calculated using the previous energy data. This value as a possible maximum should not be used because the simulation was still transient at 0.113 seconds. Once the simulation reaches

steady state the transient region will be a small if not negligible part of the overall energy consumed and power. Therefore, the data for a single point in time during the transient section should not be used to try to find possible minimum or maximum points for power loss.

This process was repeated using the oil only data shown in Figure 30. The resulting energy values are given in Table 13 and Figure 37. As in the all fluids analysis, a polynomial was fit to the data:

$$k = \frac{6.805e15x^3}{1.209e24} - \frac{8.697e14x^2}{1.476e20} + \frac{3.707e15x}{4.612e18} + \frac{6.7797e15}{7.206e16} \quad (27)$$

There are possible minima at locations closer to the gear than 39.29 mm and further than 114.29 mm.

A MATLAB code, provided in Appendix B, is used to find the maximum of the curve. Given the polynomial, a possible maximum with a clearance of 75.58 mm is found. This value is close to the clearance found for the oil and air energy consumed data.

Table 13: Single Gear Energy Consumed for Oil Only at 0.113 Seconds

Baffle Location (mm)	Baffle Clearance (mm)	Energy (J/(rad/s))
25	114.29	0.11738
50	89.29	0.12288
75	64.29	0.12290
100	39.29	0.11691

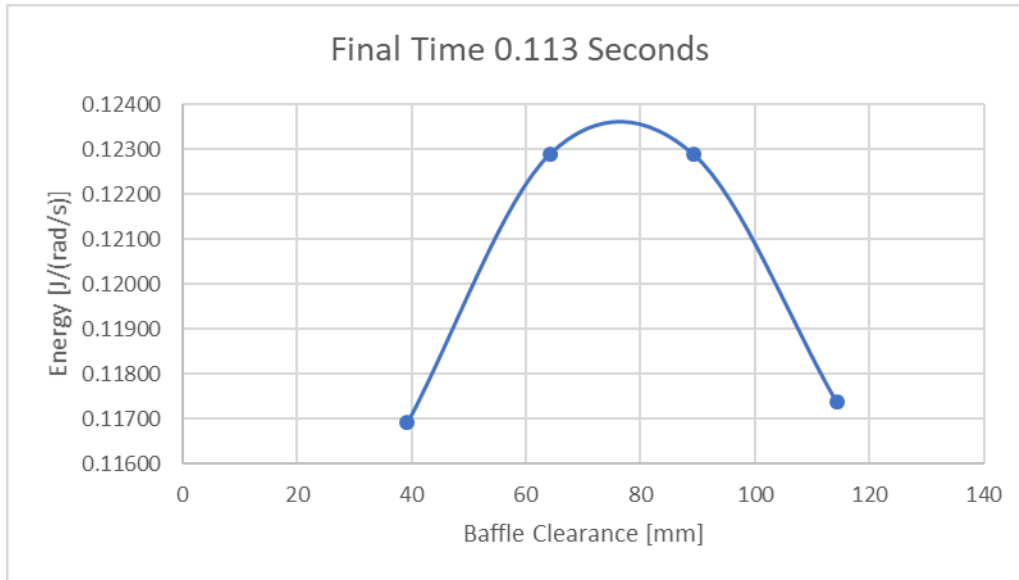


Figure 37: Single Gear Energy Consumed at 0.113 Seconds for Oil Only

It was decided to verify the possible maximum energy consumed point. For the possible maxima point there are two possibilities, a clearance of 83.29 mm from the optimization of the oil and air energy consumption data and a clearance of 75.58 mm from the optimization of the oil only energy consumption data. For this project the clearance of 83.29 mm was chosen. This clearance was chosen due to the fact that when the volume of fluid is observed as all simulations progress, the gear drags air around and creates pockets of air near the teeth, seen in Figure 38.

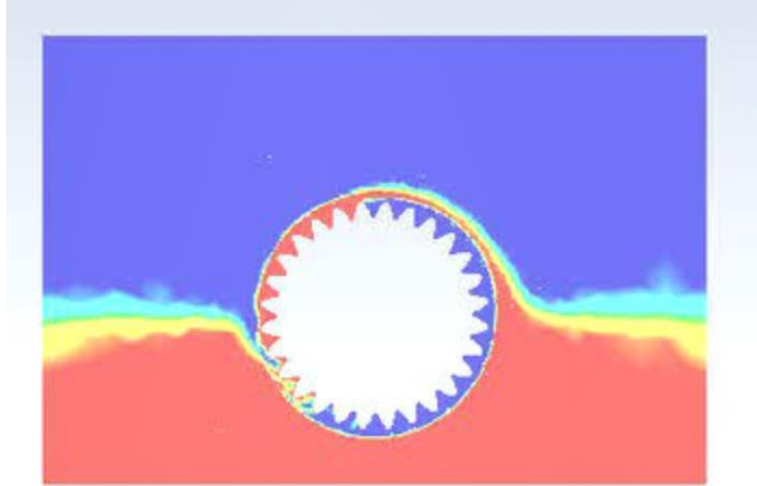


Figure 38: Volume of Fluid of Rotating Fluid with Red as Oil and Blue as Air

This means that the teeth of the gear are in as much contact with air as they are the oil, therefore data for both the air and oil must be considered. It is unknown what causes a maxima point to be in this location given the transient nature of the data. A simulation that is brought fully to steady state as well as more research would be needed to determine the exact reason why this location is a maximum. The baffle clearance for minimum energy loss is indicated to be less than 39.29 mm. Thus, a clearance of 9.29 mm was chosen as the location of interest (a baffle location of 130 mm).

When designing an optimization problem, the robustness of the optimization should be considered. Robustness of an optimization design is defined as a guarantee that the algorithm will converge starting from any initial estimate. To ensure that an optimization is robust, the function that is being optimized and the constraint equations should be defined to include uncertainties in the data.

7. Optimization Results

7.1 Optimum Baffle Location

From Chapter 6, a clearance of 83.29 mm was chosen for simulation to determine a possible maximum point, and a clearance of 9.29 mm was chosen to determine a possible minimum energy loss point. The location of these two baffles can be seen in Figure 39.

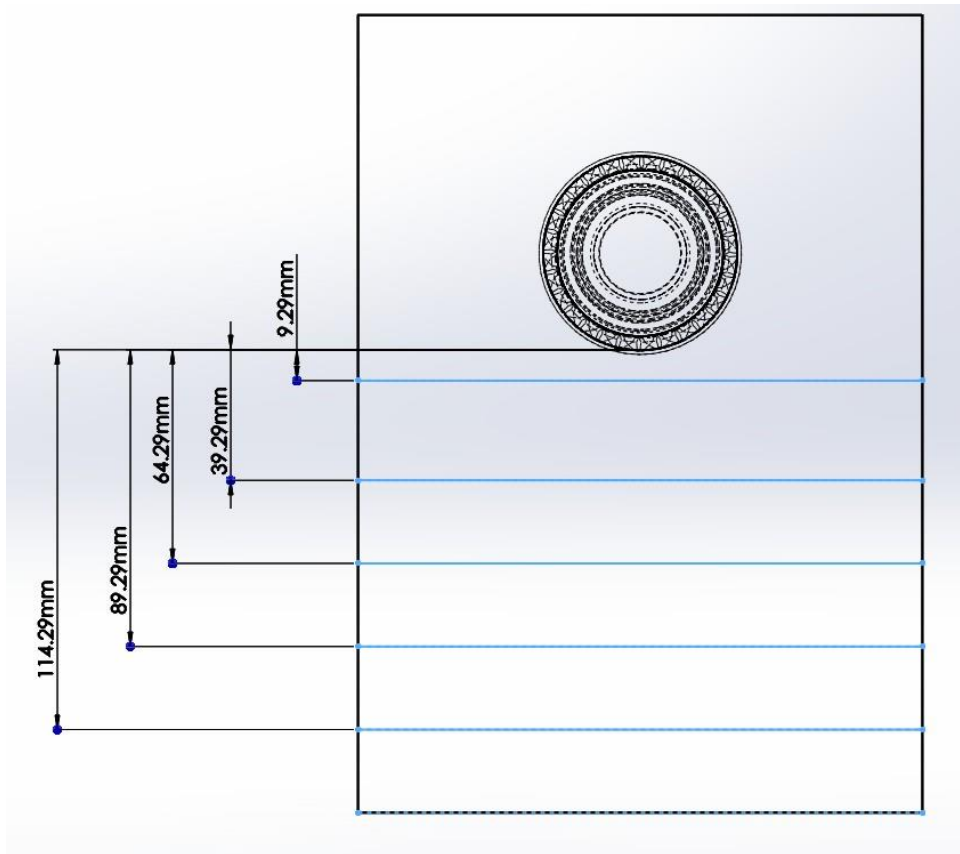


Figure 39: Location of Optimum Baffle

7.2 Torque Loss Data

Figure 40 and Figure 41 show the torque loss over time considering oil and air and oil only, respectively, for the different baffle offsets tested. It can be seen that the torque consumed by the gear with baffles of clearance 9.29 mm and 83.29 mm follows the same

pattern as that for all four of the original baffle clearances. It can also be seen that the simulations have not reached steady state.

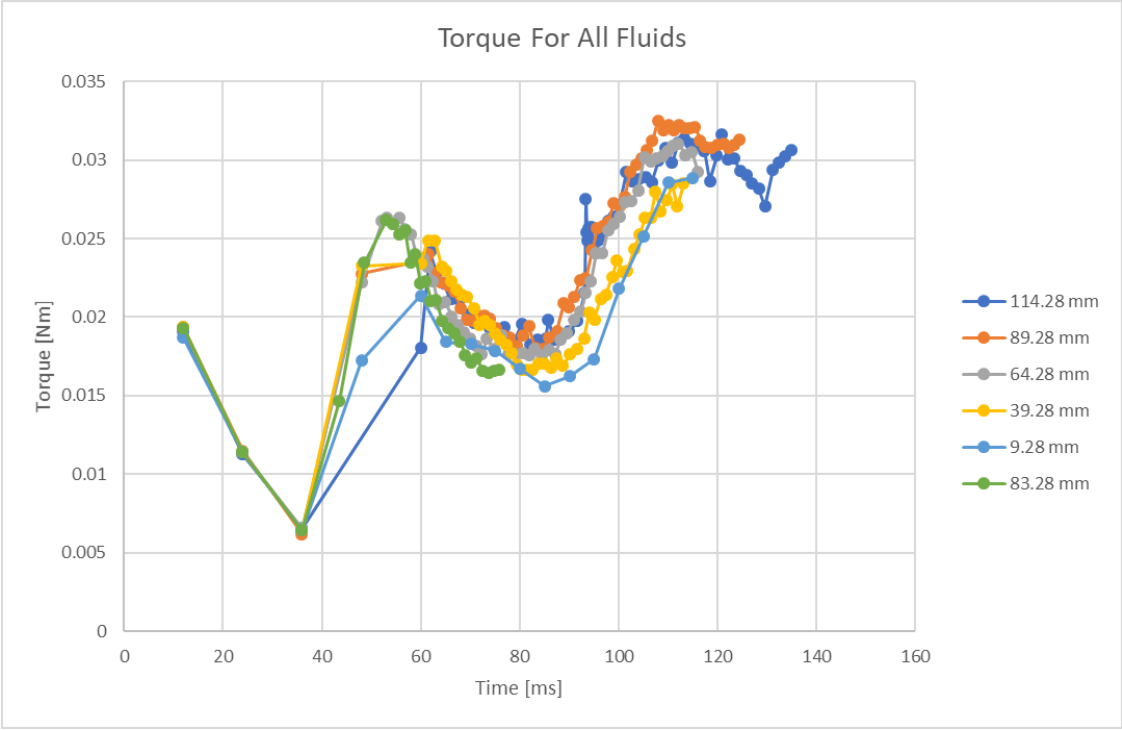


Figure 40: Torque Consumed Magnitude for all Baffle Clearances for Oil and Air

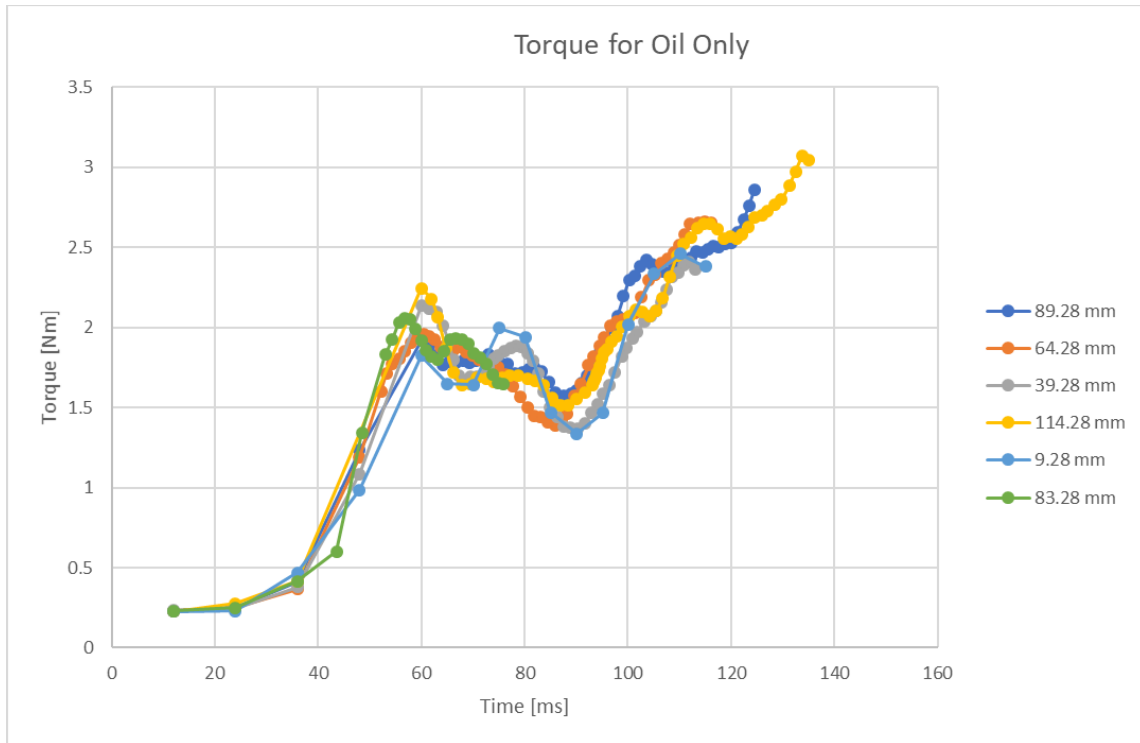


Figure 41: Torque Consumed Magnitude for all Baffle Clearances for Oil Only

7.3 Energy Consumption for Oil and Air

Due to time constraints the 83.29 mm clearance baffle simulation only reached a time of 0.0759 seconds, 1.65 rotations of the gear. The 9.29 mm clearance baffle simulation was able to reach the previous final time of 0.113 seconds. The energy consumed by the gear with the baffles here follows the same procedure used in chapter 6.1. The energy consumed by the gear for all 6 baffle locations was calculated with a stopping time of 0.0759 seconds. The results of these calculations for both oil and air can be found in Table 14 and Figure 42.

Table 14: Single Gear Energy Consumed by Air and Oil at 0.0759 Seconds

Baffle Location (mm)	Baffle Clearance (mm)	Energy (J/(rad/s))
25	114.29	0.00094
50	89.29	0.00109
56	83.29	0.00042
75	64.29	0.00111
100	39.29	0.00112
130	9.29	0.00103

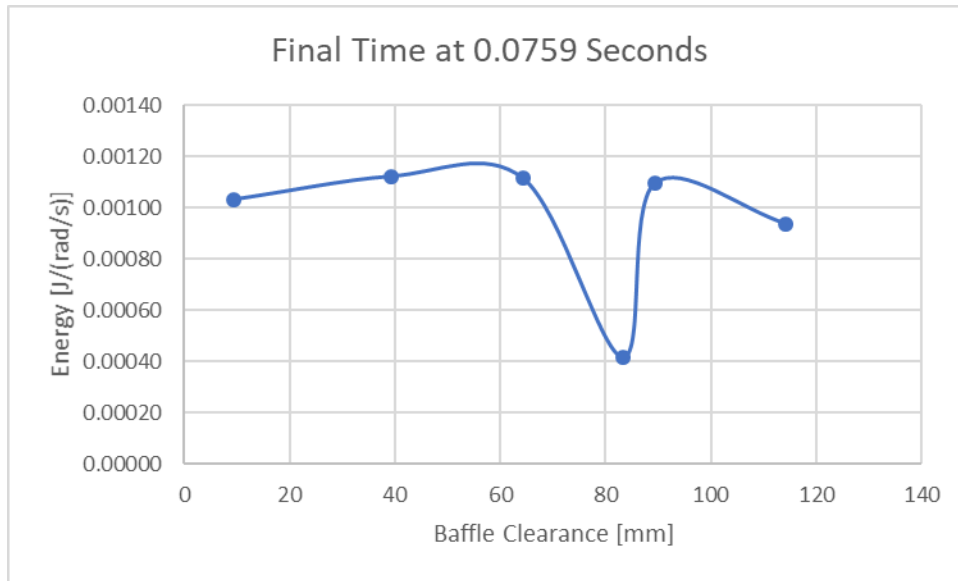


Figure 42: Single Gear Energy Consumed at 0.0759 Seconds by Air and Oil

As can be seen in Figure 42 the energy consumed by the gear with a baffle of 9.29 mm clearance consumed less energy than the 39.29 mm clearance baffle but not the 114.29 mm clearance baffle. This is consistent with results shown in Figure 34. From chapter 6.1, a baffle with a clearance less than 39.29 mm was expected to consume less energy. The simulation with a baffle of clearance 83.29 mm did not give the expected results of being a point with maximum energy consumption. This baffle clearance yielded better results than expected: less energy consumption (at 0.0759 seconds of simulation time) than the other baffles clearances.

A possible reason for this to happen is a change in how much oil is carried by the gear, as well

as how much air is kept near the teeth. These factors could change as the baffle clearance changes due to the change in the amount of oil in the gearbox.

Next, the energy consumption over 0.113 seconds was calculated for the baffle with 9.29 mm clearance. Total of the energy consumption is given in Table 15 and Figure 43.

Table 15: Single Gear Energy Consumed by Air and Oil at 0.113 Seconds

Baffle Location (mm)	Baffle Clearance (mm)	Energy (J/(rad/s))
25	114.29	0.00185
50	89.29	0.00203
56	83.29	NA
75	64.29	0.00200
100	39.29	0.00188
130	9.29	0.00011

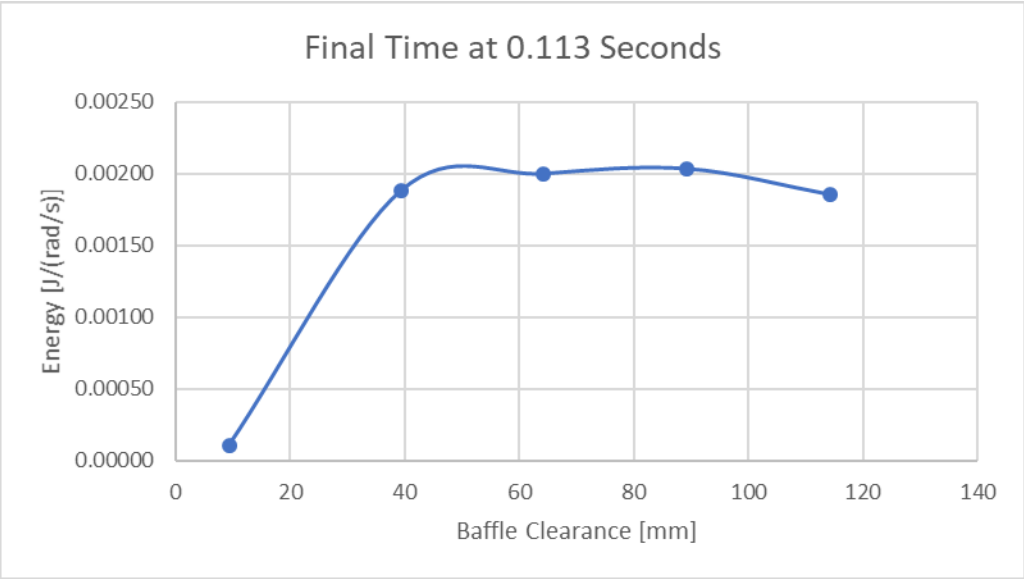


Figure 43: Energy Consumed by Air and Oil at 0.113 Seconds

From Figure 43 it can be seen that the energy consumed by gear with a 9.29 mm clearance baffle was much lower than the energy consumed by the gear with clearances of 114.29 mm, 89.29 mm, 64.29 mm and 39.29 mm.

7.4 Energy Consumption for Oil Only

The energy consumption of the gear for oil only at the 9.29 mm and 83.29 mm baffle clearances were calculated for the simulation end time of 0.0759 seconds. The energy consumption of the gear for the 9.29 mm clearance baffle was also calculated at a simulation end time of 0.113 seconds. These results are shown in Table 16 and Figure 44.

Table 16: Single Gear Energy Consumed by Oil Only at 0.0759 Seconds

Baffle Location (mm)	Baffle Clearance (mm)	Energy (J/(rad/s))
25	114.29	0.04583
50	89.29	0.04742
56	83.29	0.05148
75	64.29	0.05112
100	39.29	0.04962
130	9.29	0.04189

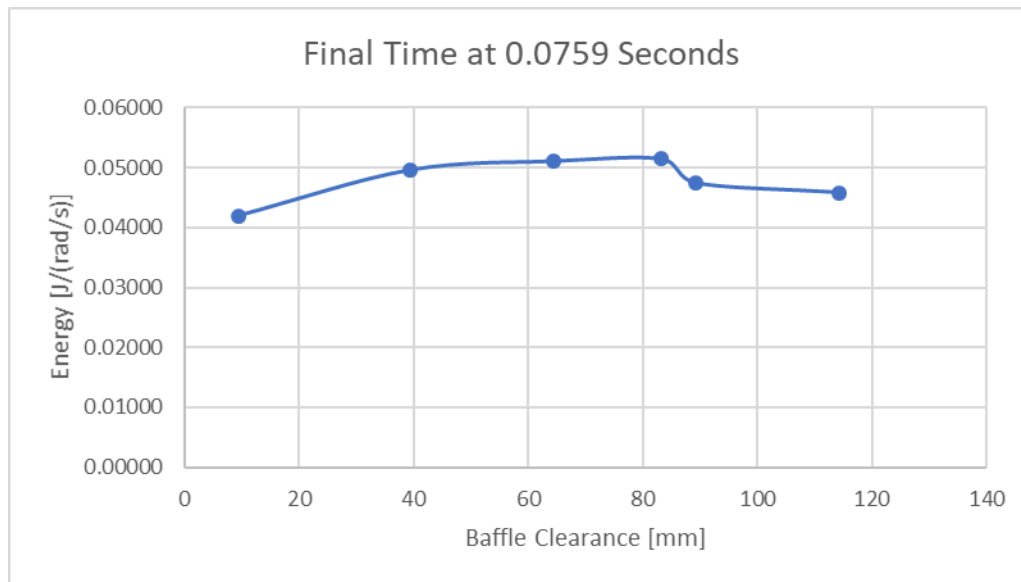


Figure 44: Single Gear Energy Consumed by Oil Only at 0.0759 Seconds

As can be seen in Figure 44 the energy consumed by the gear with a baffle of 9.29 mm clearance consumed less energy than the 39.29 mm clearance baffle and the 114.29 mm clearance baffle. This would show a minimum energy consumption point or a possible

optimum baffle location for those points tested. The simulation with a baffle of clearance 83.29 mm had a slightly higher energy consumption than the other five baffles. Which showed a slight maximum. This did not follow the same trend of the energy consumed with consideration of oil and air at the 83.29 mm clearance baffle for 0.0759 seconds, which showed a minimum energy consumption.

Table 17: Energy Consumption at 0.113 Seconds for Oil Only

Baffle Location (mm)	Baffle Clearance (mm)	Energy (J/(rad/s))
25	114.29	0.11738
50	89.29	0.12288
56	83.29	NA
75	64.29	0.12290
100	39.29	0.11691
130	9.29	0.11795

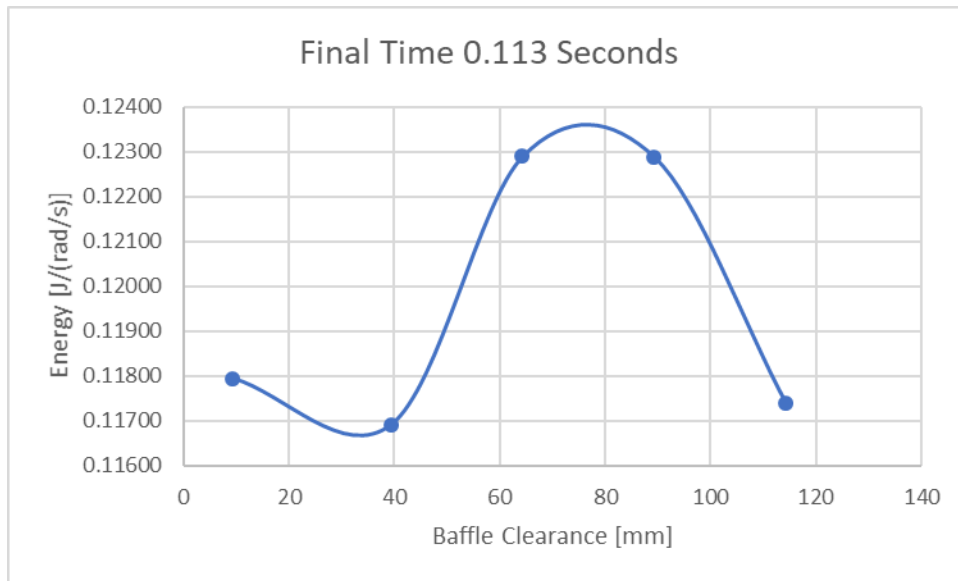


Figure 45: Single Gear Energy Consumed by Oil Only at 0.113 Seconds

Table 17 and Figure 45 give the oil only energy consumption data at 0.113 for all baffle clearances. Figure 44 shows that the energy consumed by gear with a 9.29 mm clearance baffle was not as low as the energy consumed by the gear with clearances of 114.29 mm, and 39.29

mm. This is different than the pattern found from the oil and air-based energy consumption. This discrepancy could be caused by the movement of the oil and air near the gear. If the 83.29 mm baffle clearance causes the gear to drag more air around the gear and pick up less oil or vice versa, then the data that only uses the oil information would be less accurate and would not follow the same pattern as the oil and air data. Another cause of the discrepancy could be the variability of the data due to the simulation not reaching steady-state.

8. Conclusions and Future Work

8.1 Conclusions

A process was created to identify baffle locations as possible minima or maxima energy loss points. This process was applied to board baffles in a single gear gearbox with energy loss calculated for oil effects only and with both oil and air. Initial energy loss values were found for baffle clearances of 39.29 mm, 64.29 mm, 89.29 mm, and 114.29 mm. The optimization process identified baffle clearances less than 39.29 mm as possible minima points and a clearance of 83.29 mm as a maximum energy consumption point. For clearances less than 39.29 mm, a clearance of 9.29 mm was chosen as the tested baffle clearance. It was found that at 0.113 seconds, the consumed energy for gear rotation with a baffle with a clearance of 9.29 mm was a minimum point of all five energy consumed points collected at that time. At 0.0759 seconds the energy consumed by the gear with a baffle of 9.29 mm was less than the energy consumed by the gear with baffle clearances of 39.29, 64.29 mm, and 89.29 mm, but more than clearances of 83.29 mm or 114.23 mm. Additional energy loss data for baffle clearances smaller than 39.29 and larger than 114.29 mm are needed to better identify the minimum energy loss point. Further, after 0.0759 seconds, the 83.29 mm baffle clearance energy loss data was significantly different than expected. This is likely due to the lack of steady-state data for the optimization process.

The oil and air energy loss data should be preferred over energy loss due to oil churning only or torque at a specific time for oil and air. Due to the amount of air that touches the teeth as the gear rotates the energy loss due to air cannot be ignored. Once steady state torque is reached, it will be appropriate to use torque values directly in the optimization. More baffle

clearance locations should be collected to produce a more robust optimization that better identifies minimum and maximum. The reason why certain baffle clearances result in inconsistent energy loss compared to observed trends should be further researched. The possibility of no baffle should also be investigated.

Each simulation took approximately four weeks to complete, reaching approximately 2.46 rotations when utilizing a single computer with an Intel® Core™ i7-4790 CPU @ 3.60GHz with 16.0 GB of RAM. From this observation, it can be determined that these simulations should be run on a cluster computer or using a cloud-based system to reduce the overall computing time of the simulation. By reducing the computing time, more baffle clearances can be simulated, resulting in a more robust identification of clearances that produce minimum and maximum energy loss.

8.2 Future Work

8.2.1 Expand to Steady State

This research should be expanded by allowing the simulations to reach steady state. Due to time constraints and a lack of computing power this was not possible. Once the simulations are brought to steady state, the presented optimization process can be performed. The presented simulations reached 2.46 rotations in about four weeks, which is far short of the (approximately) 15-20 rotations needed to reach steady-state, as reported in the high-fidelity Star CCM+ work. Therefore, the next step of this process should be to create a simulation that can reach steady state in a reasonable amount of time. One possible way to accomplish this would be to run the simulation with computers in parallel.

8.2.2 Expand to TGB Gearbox

Another way that this research should be expanded is by running the TGB simulation with enough computing power to complete these in a reasonable timeframe. As stated, simulations of the single-gear rotation with the present computational resources resulted in four weeks to complete approximately two and a half rotations. A two-gear system would take longer due to the increased mesh elements needed. Once implemented, results of the TGB simulations could be verified against the results of the Star CCM+ model. A similar optimization study could then be done to the TGB gearbox as was performed in this thesis for a single gear simulation.

8.2.3 Expand Optimization to Other Baffle Types

A third way that this research could be expanded is to run the simulation with different baffle designs. As shown in chapter 2, three more baffle geometries could be explored: snowman, the oval, and the semi-circle in the optimization study.

References

- [1] Concli, Franco, Carlo Gorla, Augusto Della Torre, and Gianluca Montenegro. 2015. "Churning Power Losses of Ordinary Gears: A New Approach Based on the Internal Fluid Dynamics Simulations." *Lubrication Science*, no. September: 313–26. doi:10.1002/lis.1280.
- [2] Luke, P., & Olver, A. V. (1999). A study of churning losses in dip-lubricated spur gears. *Proceedings of the Institution of Mechanical Engineers, Part G: Journal of Aerospace Engineering*, 213(5), 337–346. <https://doi.org/10.1243/0954410991533061>
- [3] Kolekar, A. S., Olver, A. V., Sworski, A. E., & Lockwood, F. E. (2014). Windage and Churning Effects in Dipped Lubrication. *Journal of Tribology*, 136(2), 21801. <https://doi.org/10.1115/1.4025992>
- [4] Hohn, Bernd-Robert, Klaus Michaelis, and Michael Hinterstoiber. 2009. "Optimization of Gearbox Efficiency."
- [5] Andersson, M. (2014). Churning losses and efficiency in gearboxes Churning losses and efficiency in gearboxes.
- [6] Petry-Johnson, T. T., Kahraman, A., Anderson, N. E., & Chase, D. R. (2008). An experimental investigation of spur gear efficiency. *Journal of Mechanical Design*, 130(6), 62601. <https://doi.org/10.1115/1.2898876>
- [7] Ariura, Y., Ueno, T., Sunaga, T., & Sunamoto, S. (1973). The Lubricant Churning Loss in Spur Gear Systems. *Bulletin of JSME*, 16(95), 881–892. <https://doi.org/10.1299/jsme1958.16.881>
- [8] Changenet, C., and P. Velex. 2008. "Housing Influence on Churning Losses in Geared Transmissions." *Journal of Mechanical Design* 130 (June 2008): 62603. doi:10.1115/1.2900714.
- [9] Arisawa, H., Nishimura, M., Imai, H., & Goi, T. (2014). Computational Fluid Dynamics Simulations and Experiments for Reduction of Oil Churning Loss and Windage Loss in Aeroengine Transmission Gears. *Journal of Engineering for Gas Turbines and Power*, 136(9), 92604. <https://doi.org/10.1115/1.4026952>
- [10] Diab, Y., Ville, F., & Velex, P. (2006). Investigations on power losses in high-speed gears. *Proceedings of the Institution of Mechanical Engineers. Part J, Journal of Engineering Tribology*, 220(3), 191–198.
- [11] Diab, Y., Ville, F., Velex, P., & Changenet, C. (2004). Windage Losses in High Speed Gears—Preliminary Experimental and Theoretical Results. *Journal of Mechanical Design*, 126(5), 903. <https://doi.org/10.1115/1.1767815>
- [12] Lord, A. A. (1998). *An Experimental Investigation of Geometric and Oil Flow Effects on Gear Windage and Meshing Losses*. University of Wales.
- [13] Zhao, N., & Jia, Q. J. (2012). Research on Windage Power Loss of Spur Gear Base on CFD. *Applied Mechanics and Materials*, 184–185, 450–455. <https://doi.org/10.4028/www.scientific.net/AMM.184-185.450>
- [14] Marchesse, Y., Changenet, C., Ville, F., & Velex, P. (2011). Investigations on CFD Simulations for Predicting Windage Power Losses in Spur Gears. *Journal of Mechanical Design*, 133(2), 24501. <https://doi.org/10.1115/1.4003357>
- [15] Gorla, C., Concli, F., Stahl, K., Höhn, B. R., Klaus, M., Schulthei, H., & Stemplinger, J. P. (2012). CFD simulations of splash losses of a gearbox. *Advances in Tribology*, 2012(1). <https://doi.org/10.1155/2012/616923>
- [16] Eastwick, C. N., & Johnson, G. (2008). Gear Windage: A Review. *Journal of Mechanical Design*,

- 130(3), 34001. <https://doi.org/10.1115/1.2829983>
- [17] Hill, M. J., & Kunz, R. F. (2012). A Computational Investigation of Gear Windage, (December).
- [18] Hill, M. J., Kunz, R. F., Medvitz, R. B., Handschuh, R. F., Long, L. N., Noack, R. W., & Morris, P. J. (2011). CFD Analysis of Gear Windage Losses: Validation and Parametric Aerodynamic Studies. *Journal of Fluids Engineering*, 133(3), 31103. <https://doi.org/10.1115/1.4003681>
- [19] Handschuh, R. F., & Glenn, N. (2010). Initial Experiments of High-Speed Drive System Windage Losses. *International Conference on Gears*, (November), 1–13.
- [20] Kunz, R. F., Hill, M. J., Schmehl, K. J., & McIntyre, S. M. (2012). Computational studies of the roles of shrouds and multiphase flow in high speed gear windage loss. *Annual Forum Proceedings - AHS International*, 3.
- [21] Winfree, D. D. (2014). Detc2013-13039 Reducing Gear Windage Losses From High Speed Gears and, 1–16.
- [22] Johnson, G., Chandra, B., Foord, C., & Simmons, K. (2009). Windage Power Losses From Spiral Bevel Gears With Varying Oil Flows and Shroud Configurations. *Journal of Turbomachinery*, 131(4), 41019. <https://doi.org/10.1115/1.3072519>
- [23] Johnson, G., Simmons, K., & Foord, C. (2007). Experimental investigation into windage power loss from a shrouded spiral bevel gear. In *Proceedings of the ASME Turbo Expo 2007: Power for Land, Sea and Air* (Vol. 6, pp. 57–66).
- [24] Rapley, S., Eastwick, C., & Simmons, K. (2007). The application of CFD to model windage loss from a spiral bevel gear. In *Proceedings of the ASME Turbo Expo 2007* (Vol. 6, pp. 47–56).
- [25] Rapley, S., Eastwick, C., & Simmons, K. (2008). Effect of variations in shroud geometry on single phase flow over a shrouded single spiral gear. In *Proceedings of the ASME Turbo Expo 2008: Power for Land, Sea and Air* (pp. 1483–1492).
- [26] Farrall, M., Simmons, K., Hibberd, S., & Young, C. (2005). Computational Investigation of the Airflow Through a Shrouded Bevel Gear. *ASME Conference Proceedings*, 2005(47268), 1259–1265. <https://doi.org/10.1115/GT2005-68879>
- [27] Boness, R. J. (1989). Churning losses of discs and gears running partially submerged in oil. In *proceedings of the 1989 international power transmission and gearing conference, held in Chicago, Illinois, April 25-28, 1989: new technologies for p* (pp. 355–359).
- [28] [Digital image]. (n.d.). Retrieved from <https://mechanicalendeavour.wordpress.com/2011/03/15/gear-basics/>
- [29] Terekhov, A. S. (1975). Hydraulic Losses in Gearboxes with oil immersion. *Russian Engineering Journal*, 55(5), 7–11.
- [30] Shimokawa, Yohei. 2013. “Technology Development to Improve Jatco CVT8 Efficiency.” doi:10.4271/2013-01-0364.
- [31] Chen, Sheng-Wei, and Susumu Matsumoto. 2016. “Influence of Relative Position of Gears and Casing Wall Shape of Gear Box on Churning Loss under Splash Lubrication Condition—Some New Ideas.” [Http://Dx.Doi.Org/10.1080/10402004.2015.1129568](http://Dx.Doi.Org/10.1080/10402004.2015.1129568) 2004 (June). Taylor & Francis: 993–1004. doi:10.1080/10402004.2015.1129568.
- [32] Gorla, Carlo, Franco Concli, Karsten Stahl, Bernd Robert Höhn, Klaus Michaelis, Hansjörg Schultheiß, and Johann Paul Stemplinger. 2013. “Hydraulic Losses of a Gearbox: CFD Analysis and Experiments.” *Tribology International* 66: 337–44. <https://doi.org/10.1016/j.triboint.2013.06.005>.
- [33] Kraetschmer, M., Kodela, C., Loss, C., Transmission, M., Box, G., & Cfd, U. (2015). Churning Loss Estimation for Manual Transmission Gear Box Using CFD General Motors Technical Center India Chandrasekhar Kodela, (Figure 1). <https://doi.org/10.4271/2015-26-0201>
- [34] Seetharaman, S., A. Kahraman, M. D. Moorhead, and T. T. Petry-Johnson. 2009. “Oil Churning

- Power Losses of a Gear Pair: Experiments and Model Validation." *Journal of Tribology* 131 (2): 22202. doi:10.1115/1.3085942.
- [35] Seetharaman, S., and A. Kahraman. 2009. "Load-Independent Spin Power Losses of a Spur Gear Pair: Model Formulation." *Journal of Tribology* 131 (2): 22201. doi:10.1115/1.3085943.
- [36] Desai, Kaushik. 2013. "Oil Churning Losses in Automatic Transmission."
- [37] Michaelis, Klaus, Bernd-Robert Höhn, and Michael Hinterstoißer. 2011. "Influence Factors on Gearbox Power Loss." *Industrial Lubrication and Tribology* 63 (1): 46–55. doi:10.1108/00368791111101830.
- [38] Polly, Joseph H. 2013. "An Experimental Investigation of Churning Power Losses of a Gearbox." The Ohio State University.
- [39] Yang Yang, William W. Liou, 2018, privation communication, Western Michigan University, Kalamazoo, Michigan, (2018).
- [40] Yang Yang, William W. Liou, 2018, privation communication, Western Michigan University, Kalamazoo, Michigan, (2019).
- [41] Ansys Fluent 12.0 User's Guide -6.2.2 Mesh Quality. (n.d.). Retrieved from <https://www.afs.enea.it/project/neptunius/docs/fluent/html/ug/node167.htm>.
- [42] Mesh Quality. (2015, June 29). Retrieved from https://www.sharcnet.ca/Software/Ansys/16.2.3/en-us/help/flu_ug/flu_ug_mesh_quality.html
- [43] Caeai.com. (2019). *Generating Inflation Layers for CFD - ANSYS e-Learning | CAE Associates*. [online] Available at: <https://caeai.com/resources/generating-inflation-layers-cfd-ansys-e-learning> [Accessed 22 Apr. 2019].
- [44](n.d.). Retrieved from <https://www.sharcnet.ca/Software/Fluent6/html/ug/node986.htm>
- [45] Dimensionless wall distance (y plus). (n.d.). Retrieved from [https://www.cfd-online.com/Wiki/Dimensionless_wall_distance_\(y_plus\)](https://www.cfd-online.com/Wiki/Dimensionless_wall_distance_(y_plus)).
- [46] Zou, Y., Zhao, X., & Chen, Q. (2017). Comparison of STAR-CCM and ANSYS Fluent for simulating indoor airflows. *Building Simulation*, 11(1), 165-174. doi:10.1007/s12273-017-0378-8
- [47] Afs.enea.it. (2019). *ANSYS FLUENT 12.0 User's Guide - The Contents of This Manual*. [online] Available at: <http://www.afs.enea.it/project/neptunius/docs/fluent/html/ug/node3.htm> [Accessed 4 Apr. 2019].
- [48] Atresh, A. (n.d.). Tips & Tricks: Convergence and Mesh Independence Study. Retrieved from <https://www.computationalfluidynamics.com.au/convergence-and-mesh-independent-study/>.
- [49] Eureka.im. (n.d.). Retrieved from <http://www.eureka.im/4501.html>.

Appendices

Appendix A:

Energy Oil and Air MATLAB File

```

clc
clear all
close all
%import the power data
m= readmatrix('torque all fluids 56 correct.xlsx','Sheet',2, 'Range', 'B2:B5');

torqueall= m.';
%create vectors of the data set

x = [114.29,89.29,64.29,39.29]
y = abs(torqueall)

%create an estimate function of the data and plot the data points
coeefs = polyfit(x, y, length(y)-1)
plot (x, y, 'ro', 'MarkerSize', 10);

%interpolate the data and plot so that the estimate function can be seen
interpolatedx = linspace(min(x), max(x),500);
interpolatedy = polyval (coeefs, interpolatedx);
hold on;
plot(interpolatedx, interpolatedy, 'b-', 'Linewidth', 3);
grid on;
title('Interpolating Polynomial', 'FontSize', 10);
xlabel('x', 'FontSize', 10);
ylabel('y', 'FontSize', 10);

%differentiate the polynomial
q = polyder(coeefs);
%create a symbolic variable
syms t
assume(t, 'real')
assumeAlso(t>0)
%create a symbolic polynomial from the coefficients found by estimation
k = poly2sym(coeefs,t)

%create a function handle from symbolic polynomial
poly = matlabFunction(k);

%create symbolic polynomial and function handle for first differential of
%estimation

h= poly2sym(q,t)
v = matlabFunction(h);
%find the t values that cause the first differential to be equal to zero
%a necessary condition of optimization

n= vpasolve(h == 0,t);

% define the error allowed for how close to zero the slope can be

```

```

e=0.00001;

for i = 1:length(n) % this will be done for each number in the vector of solution that cause the
first differential to equal zero
    if (n(i)>=0) %only use values with a zero slope if they are above 0 because of physical
constraints
        disp(n(i)) % display the value of t
        b=n(i);
        if (abs(v(b)-0)<=e) % if the value of t causes the defierential to be approximately
equal to zero
            disp('satisfies necessary condition')
            z = polyder(q); % find the second differential
            m = poly2sym(z,t); %symbolic polynomial
            l=matlabFunction(m); %function handle
            if (l(b)>0) % find out if the t value causes the second differential to be greater
than zero which is the suffeciency condition
                disp('satisfies the suffeciency condition')
            else
                disp('doesnt satisfy the suffeciency condition')
            end
        else
            disp('doesnt satisfy the necessary condition')
        end
    end
end
end

```

x =

114.2900 89.2900 64.2900 39.2900

y =

0.0019 0.0020 0.0020 0.0019

coefs =

-0.0000 0.0000 -0.0000 0.0018

k =

- (6717458543513849*t^3)/4835703278458516698824704 +
(3785907283434641*t^2)/18889465931478580854784 - (5473222059833393*t)/1180591620717411303424 +
8482806861262233/4611686018427387904

h =

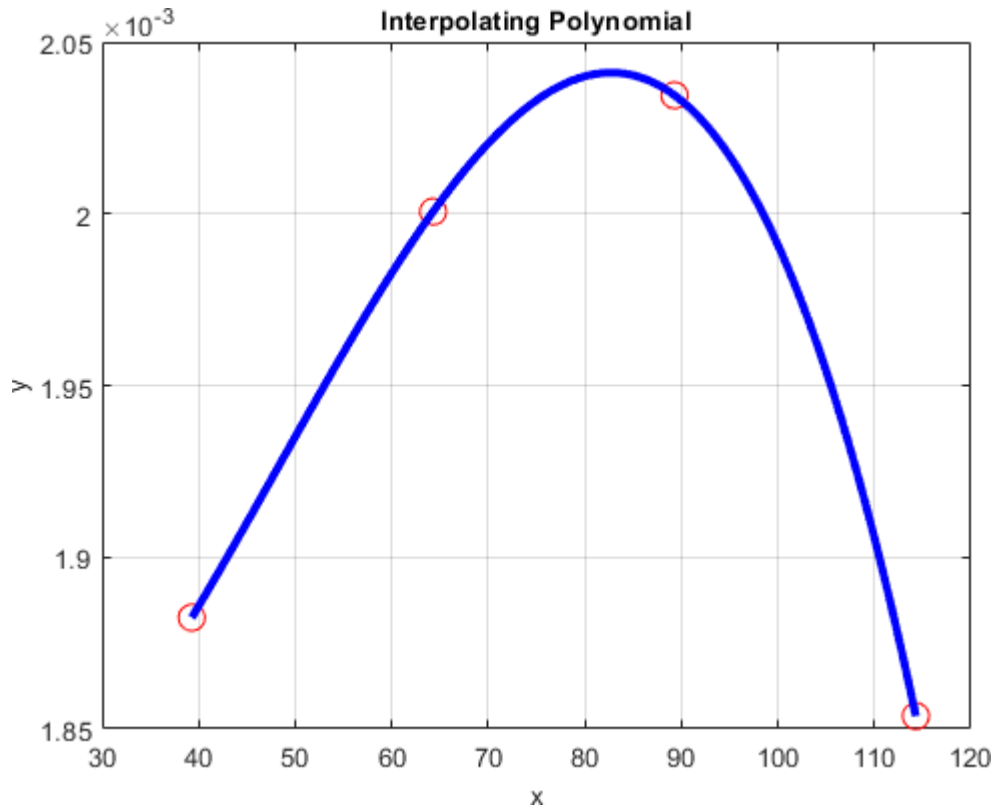
(3785907283434641*t)/9444732965739290427392 - (5038093907635387*t^2)/1208925819614629174706176 -

5473222059833393/1180591620717411303424

13.444744148156863325899770210217

satisfies necessary condition
satisfies the sufficiency condition
82.741659115429318532373354405366

satisfies necessary condition
doesnt satisfy the sufficiency condition



Published with MATLAB® R2019a

Appendix B:

Energy Oil only MATLAB File

```

clc
clear all
close all
%import the power data
m= readmatrix('torque oil only 56 correct.xlsx','Sheet',2, 'Range', 'H2:H5');

torqueoil= m.';
%create vectors of the data set

x = [114.29,89.29,64.29,39.29]
y = abs(torqueoil)

%create an estimate function of the data and plot the data points
coeefs = polyfit(x, y, length(y)-1)
plot (x, y, 'ro', 'MarkerSize', 10);

%interpolate the data and plot so that the estimate function can be seen
interpolatedx = linspace(min(x), max(x),500);
interpolatedy = polyval (coeefs, interpolatedx);
hold on;
plot(interpolatedx, interpolatedy, 'b-', 'Linewidth', 3);
grid on;
title('Interpolating Polynomial', 'FontSize', 10);
xlabel('x', 'FontSize', 10);
ylabel('y', 'FontSize', 10);

%differentiate the polynomial
q = polyder(coeefs);
%create a symbolic variable
syms t
assume(t, 'real')
assumeAlso(t>0)
%create a symbolic polynomial from the coefficients found by estimation
k = poly2sym(coeefs,t)

%create a function handle from symbolic polynomial
poly = matlabFunction(k);

%create symbolic polynomial and function handle for first differential of
%estimation

h= poly2sym(q,t)
v = matlabFunction(h);
%find the t values that cause the first differential to be equal to zero
%a necessary condition of optimization

n= vpasolve(h == 0,t);

% define the error allowed for how close to zero the slope can be

```

```

e=0.00001;

for i = 1:length(n) % this will be done for each number in the vector of solution that cause the
first differential to equal zero
    if (n(i)>=0) %only use values with a zero slope if they are above 0 because of physical
constraints
        disp(n(i)) % display the value of t
        b=n(i);
        if (abs(v(b)-0)<=e) % if the value of t causes the defierential to be approximately
equal to zero
            disp('satisfies necessary condition')
            z = polyder(q); % find the second differential
            m = poly2sym(z,t); %symbolic polynomial
            l=matlabFunction(m); %function handle
            if (l(b)>0) % find out if the t value causes the second differential to be greater
than zero which is the suffeciency condition
                disp('satisfies the suffeciency condition')
            else
                disp('doesnt satisfy the suffeciency condition')
            end
        else
            disp('doesnt satisfy the necessary condition')
        end
    end
end
end
end

```

x =

114.2900 89.2900 64.2900 39.2900

y =

0.1174 0.1229 0.1229 0.1169

coefs =

0.0000 -0.0000 0.0008 0.0941

k =

$(6804844307453777*t^3)/1208925819614629174706176 - (869682960809801*t^2)/147573952589676412928$
 $+ (3706948439561677*t)/4611686018427387904 + 6779669146142839/72057594037927936$

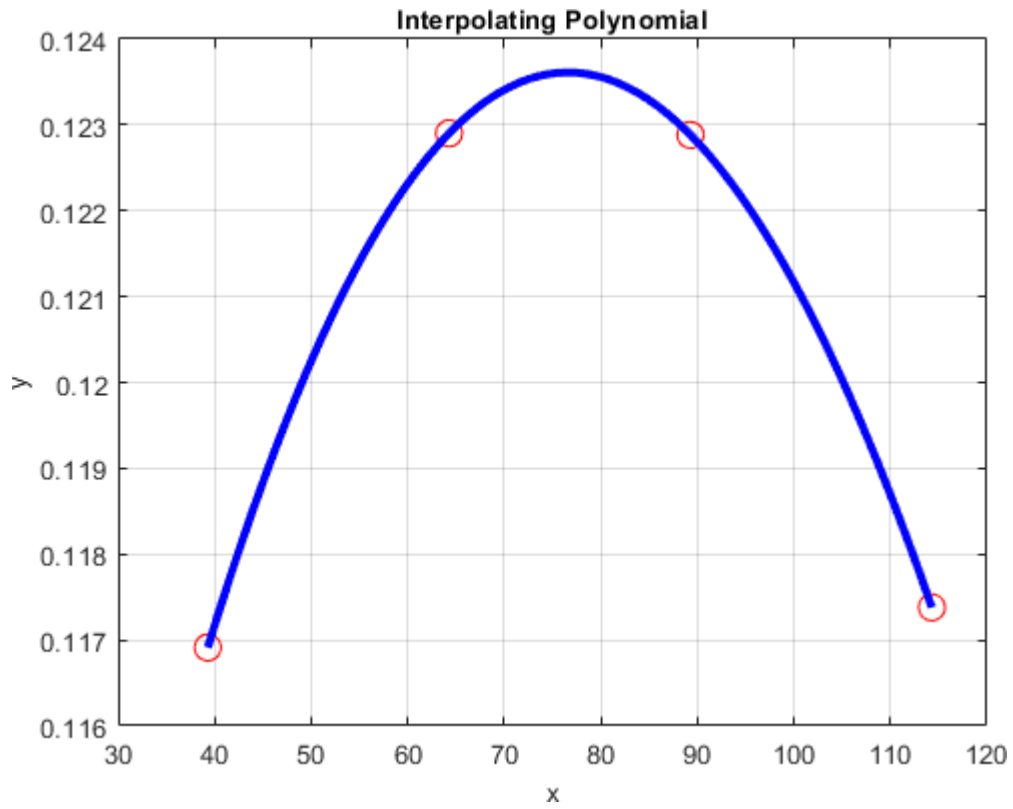
h =

$(5103633230590333*t^2)/302231454903657293676544 - (869682960809801*t)/73786976294838206464 +$
 $3706948439561677/4611686018427387904$

76.606577436612250541451928558412

satisfies necessary condition
doesn't satisfy the sufficiency condition
621.37097042587506150971094029353

satisfies necessary condition
satisfies the sufficiency condition



Published with MATLAB® R2019a

Appendix C:

Torque Oil and Air at 0.113 Seconds MATLAB Code

```

clc
clear all
close all
%import the power data
m= readmatrix('torque all fluids 56 and 130 correct.xlsx','Sheet',1, 'Range', 'AK41:AK44');

torqueall= m.';
%create vectors of the data set

x = [114.29,89.29,64.29,39.29]
y = abs(torqueall)

%create an estimate function of the data and plot the data points
coefs = polyfit(x, y, length(y)-1)
plot (x, y, 'ro', 'MarkerSize', 10);

%interpolate the data and plot so that the estimate function can be seen
interpolatedx = linspace(min(x), max(x),500);
interpolatedy = polyval (coefs, interpolatedx);
hold on;
plot(interpolatedx, interpolatedy, 'b-', 'Linewidth', 3);
grid on;
title('Interpolating Polynomial', 'FontSize', 10);
xlabel('x', 'FontSize', 10);
ylabel('y', 'FontSize', 10);

%differentiate the polynomial
q = polyder(coefs);
%create a symbolic variable
syms t
assume(t, 'real')
assumeAlso(t>0)
%create a symbolic polynomial from the coefficients found by estimation
k = poly2sym(coefs,t)

%create a function handle from symbolic polynomial
poly = matlabFunction(k);

%create symbolic polynomial and function handle for first differential of
%estimation

h= poly2sym(q,t)
v = matlabFunction(h);
%find the t values that cause the first differential to be equal to zero
%a necessary condition of optimization

n= vpasolve(h == 0,t);

% define the error allowed for how close to zero the slope can be

```

```

e=0.00001;

for i = 1:length(n) % this will be done for each number in the vector of solution that cause the
first differential to equal zero
    if (n(i)>=0) %only use values with a zero slope if they are above 0 because of physical
constraints
        disp(n(i)) % display the value of t
        b=n(i);
        if (abs(v(b)-0)<=e) % if the value of t causes the defierential to be approximately
equal to zero
            disp('satisfies necessary condition')
            z = polyder(q); % find the second differential
            m = poly2sym(z,t); %symbolic polynomial
            l=matlabFunction(m); %function handle
            if (l(b)>0) % find out if the t value causes the second differential to be greater
than zero which is the suffeciency condition
                disp('satisfies the suffeciency condition')
            else
                disp('doesnt satisfy the suffeciency condition')
            end
        else
            disp('doesnt satisfy the necessary condition')
        end
    end
end
end

```

x =

114.2900 89.2900 64.2900 39.2900

y =

0.0314 0.0320 0.0303 0.0285

coefs =

-0.0000 0.0000 -0.0002 0.0306

k =

- (7066087919170841*t^3)/302231454903657293676544 + (5193538186097541*t^2)/1180591620717411303424
- (3521539741885321*t)/18446744073709551616 + 8826614766467045/288230376151711744

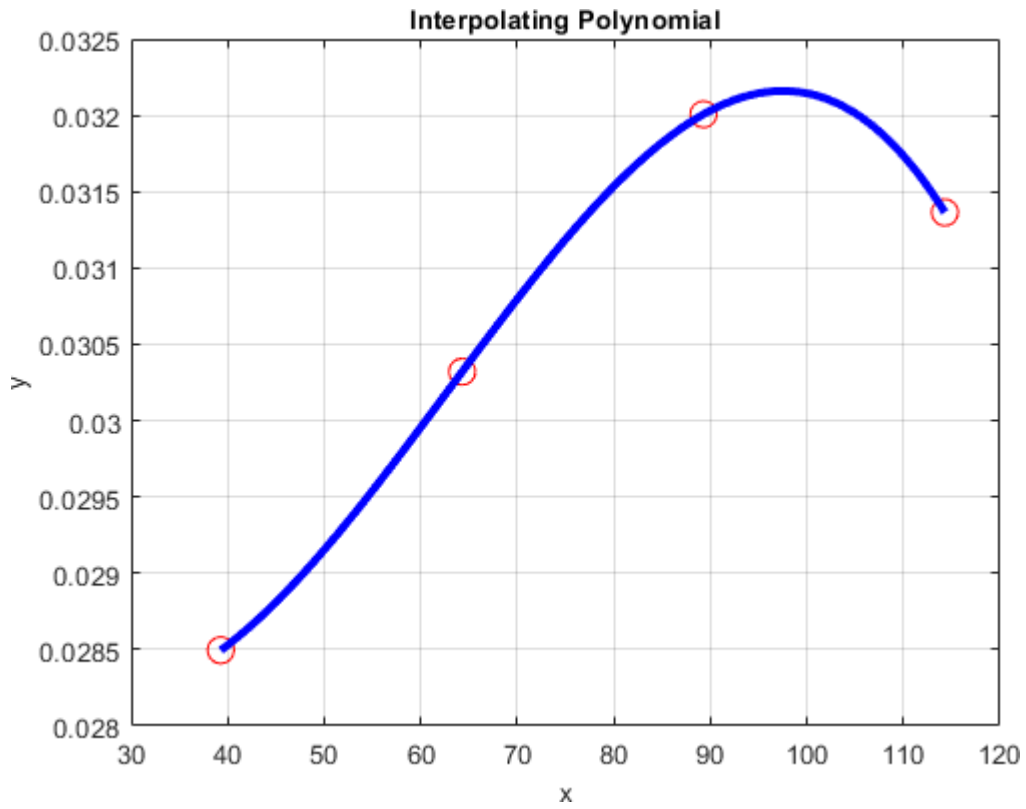
h =

(5193538186097541*t)/590295810358705651712 - (5299565939378131*t^2)/75557863725914323419136 -
3521539741885321/18446744073709551616

27.906228144530346979623470383851

satisfies necessary condition
satisfies the sufficiency condition
97.532891856020480795457019079341

satisfies necessary condition
doesnt satisfy the sufficiency condition



Published with MATLAB® R2019a

Appendix D:

Torque Oil Only at 0.113 Seconds MATLAB Code

```

clc
clear all
close all
%import the power data
m= readmatrix('torque oil only 56 and 130 correct.xlsx','Sheet',1, 'Range', 'AI32:AI35');

torqueoil= m.';
%create vectors of the data set

x = [114.29,89.29,64.29,39.29]
y = abs(torqueoil)

%create an estimate function of the data and plot the data points
coeefs = polyfit(x, y, length(y)-1)
plot (x, y, 'ro', 'MarkerSize', 10);

%interpolate the data and plot so that the estimate function can be seen
interpolatedx = linspace(min(x), max(x),500);
interpolatedy = polyval (coeefs, interpolatedx);
hold on;
plot(interpolatedx, interpolatedy, 'b-', 'Linewidth', 3);
grid on;
title('Interpolating Polynomial', 'FontSize', 10);
xlabel('x', 'FontSize', 10);
ylabel('y', 'FontSize', 10);

%differentiate the polynomial
q = polyder(coeefs);
%create a symbolic variable
syms t
assume(t, 'real')
assumeAlso(t>0)
%create a symbolic polynomial from the coefficients found by estimation
k = poly2sym(coeefs,t)

%create a function handle from symbolic polynomial
poly = matlabFunction(k);

%create symbolic polynomial and function handle for first differential of
%estimation

h= poly2sym(q,t)
v = matlabFunction(h);
%find the t values that cause the first differential to be equal to zero
%a necessary condition of optimization

n= vpasolve(h == 0,t);

% define the error allowed for how close to zero the slope can be

```

```

e=0.00001;

for i = 1:length(n) % this will be done for each number in the vector of solution that cause the
first differential to equal zero
    if (n(i)>=0) %only use values with a zero slope if they are above 0 because of physical
constraints
        disp(n(i)) % display the value of t
        b=n(i);
        if (abs(v(b)-0)<=e) % if the value of t causes the defierential to be approximately
equal to zero
            disp('satisfies necessary condition')
            z = polyder(q); % find the second differential
            m = poly2sym(z,t); %symbolic polynomial
            l=matlabFunction(m); %function handle
            if (l(b)>0) % find out if the t value causes the second differential to be greater
than zero which is the suffeciency condition
                disp('satisfies the suffeciency condition')
            else
                disp('doesnt satisfy the suffeciency condition')
            end
        else
            disp('doesnt satisfy the necessary condition')
        end
    end
end
end
end

```

x =

114.2900 89.2900 64.2900 39.2900

y =

2.6180 2.4737 2.6522 2.3629

coefs =

0.0000 -0.0020 0.1496 -0.9391

k =

$(4978065816292351*t^3)/590295810358705651712 - (72084186138651*t^2)/36028797018963968 +$
 $(5391074311360521*t)/36028797018963968 - 8458781146343701/9007199254740992$

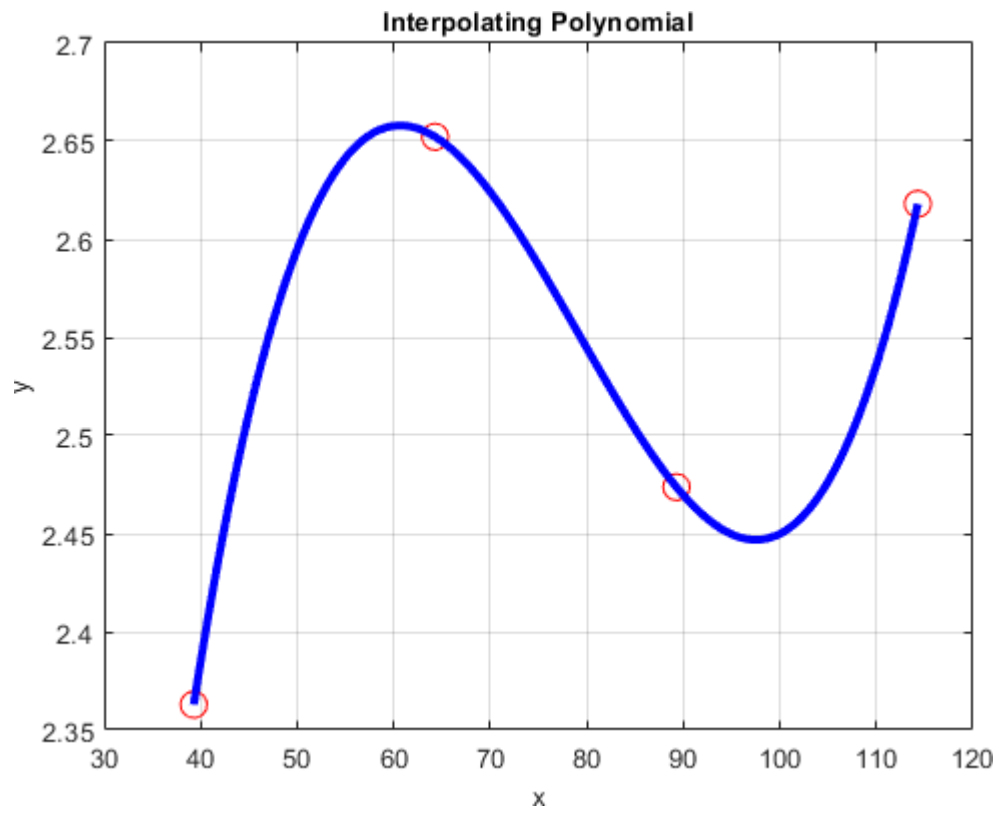
h =

$(3733549362219263*t^2)/147573952589676412928 - (72084186138651*t)/18014398509481984 +$
 $5391074311360521/36028797018963968$

60.655517720860920575749112626711

satisfies necessary condition
doesn't satisfy the sufficiency condition
97.508629999639860760474676981745

satisfies necessary condition
satisfies the sufficiency condition



Published with MATLAB® R2019a

Appendix E:

Parallel vs. Serial Computing

When using a solver to compute simulation results an option of running the solution in serial or in parallel is given. A serial solution will be calculated using only one core of one computer, and every calculation will be done one at a time. A parallel solution can be done in multiple ways. There is same computer parallel and multicomputer parallel. Same computer parallel will use multiple cores on the same computer to solve multiple simulation equations concurrently. A multi computer parallel system will still use multiple cores to solve the simulation equations concurrently, but the cores do not need to be part of the same machine. The serial solution is easier to converge than the parallel solution, this is due to the higher complexity of the parallel solution. Even though the serial solution is easier to converge, the parallel solution is less time consuming. Parallel computing is less time consuming because there are multiple computers or multiple cores solving the equations concurrently, allowing the simulation to complete in less time.